

**SYNTHESIS AND ACTIVATION OF MESOPOROUS CARBONS WITH
TUNABLE NITROGEN CONTENT FOR SUPERCAPACITOR ELECTRODES**

A Thesis

Presented to the Faculty of the Graduate School

of Cornell University

In Partial Fulfillment of the Requirements for the Degree of

Master of Science

by

Mian Pan

August 2016

© 2016 Mian Pan

ABSTRACT

Mesoporous carbons are excellent materials for supercapacitor electrodes due to their high surface areas, tunable porosity, good electrical conductivity, and low cost. Doping of nitrogen in mesoporous carbons can enhance their capacitance. To date, three strategies for preparation of nitrogen-doped mesoporous carbons have been developed: post-synthesis modification methods, hard templating, and soft templating approaches. In this work, we present a novel and cost effective strategy to synthesize nitrogen-doped mesoporous carbons possessing large surface area, uniform porosity with high and tunable (~ 2 -22 at. %) nitrogen doping via an ice-templating approach from cyanamide, sucrose and colloidal silica. An iodine pretreatment can be applied to further increase the nitrogen content in the final carbon materials. These doped carbons exhibited high specific capacitance of up to 238 F g⁻¹ with good capacity retention at high rates (up to 80% at 25A/g). In addition, CO₂ activation of the obtained carbons can produce higher specific surface area (up to 1998m²/g) and larger pore volume (up to 2.98cm³/g) materials. The activated nitrogen doped carbon possessed a large fraction of fine micropores with fair nitrogen and oxygen dopant leading to superior capacity (up to 316F/g), good capacity retention at high rates (220F/g at 25A/g) and long-term cycle stability (98% retention after 600 cycle).

BIOGRAPHICAL SKETCH

Mian Pan was born and raised in China, in the city of Lianyungang. She was the only child of her parents. As most other Chinese students, Mian focused mainly on study at a young age and she was especially good at math. Her initial interest in materials science stemmed from her attendance at Youth Science & Technology Camp during the summer of Grade 10th. It was the first time Mian heard and saw how polymer materials and functional materials have dramatically improved people's lives. Afterwards, Mian dreamed of specializing in chemistry and material science during her undergraduate studies.

Then she was admitted to Nanjing University (NJU), one of the top 5 universities in China, at her age of 18. As student at the School of Chemistry and Chemical Engineering, Mian was equipped with a solid foundation of theoretical knowledge and experimental skills, coupled with lots of experience gained in the intensive training of the polymer materials synthesis and material performance testing. For example, in April 2012, she had the first opportunity to take charge of a formal research project, Transient Meso-morphic Transitions in Polymers Studied by Fast Scanning Calorimetry Combined with Raman Spectroscopy. As team leader, Mian chose this project independently and it was assessed as a national innovation program because of its innovation and feasibility, hence she was granted with 20,000 yuan of project fund. Mian was also very interested in research topics about application of materials and she worked on synthesizing electrode materials for electrochemical capacitor as graduation project in Prof. Xizhang Wang's research group.

After graduation from NJU, Mian came alone to USA to pursue graduate studies of materials science in Cornell University. At Cornell, Mian joined Professor Emmanuel P. Giannelis's research group. During her two year master's program, many friendly senior

graduate students and post docs in this group had helped her a lot. Also, she was greatly inspired by her advisor that encouraged her scientific curiosity. Her work in Cornell was focused on synthesizing N-doped mesoporous carbon for supercapacitor electrodes. This project gave her an ability to utilize scientific advances to make superior materials for energy storage device and led to her later job in GE.

Now, Mian has come back to China. She really lived a wonderful life in Cornell and she will miss her friends in Ithaca. For her future, Mian will strive to learn better about how to apply her professional knowledge of materials into practice use and she is considering to seek for opportunity to continue her study in a PHD degree two or three years later.

Dedicated to all the people who have helped me in Cornell and also to my parents: for
always encouraging me, supporting me, and trusting me.

ACKNOWLEDGMENTS

First, I want to express my deepest gratitude to my parents, Enjun Pan and Jiajuan Wang, for their love, patience, trust and their great support in my life. Their kindness, intelligence and humility has always inspired me to be a better person.

I would also like to acknowledge my advisor, Emmanuel, who gave me his expert advice, support and encouragement during my two years study in Cornell. I was very lucky to be his student and to work in his group. I have learned a lot from him and his guidance is immensely appreciated.

To my committee member, Professor Van Dover, thank you for being on my committee, despite your busy schedules.

To my collaborators to this work presented in this thesis, Ritu and Turki, thank you for always willing to help me solve problems in the lab as well as provide valuable advice in my life.

To all group members, you are all incredibly skillful people and it was very pleasant to work with you all.

TABLE OF CONTENTS

Biographical Sketch.....	iv
Dedication.....	vi
Acknowledgements.....	vii
Table of Contents.....	viii
List of Figures.....	x
List of Tables.....	xiii
1.INTRODUCTION	1
1.1 Introduction to Supercapacitors.....	1
1.2 Introduction to Mesoporous Carbon.....	5
1.3 Functionalization of Mesoporous Carbon	6
1.4 Nitrogen Doping of Carbons	6
1.5 Synthesis Methods of Nitrogen Doped Mesoporous Carbon	8
1.5.1 Post-Synthesis Modification Methods.....	8
1.5.2 Hard Templating Methods.....	10
1.5.3 Soft Templating Methods	12
1.6 Previous Work on Mesoporous Carbon in Our Group	13
REFERENCES	17
2.DESIGN AND SYTHESIS OF MESOPOROUS CARBONS WITH TUNABLE AMOUNT OF NITROGEN DOPING	23
2.1 Introduction	23
2.2 Experimental Section.....	24
2.2.1 Materials	24
2.2.2 Synthesis Procedure of Nitrogen Doped Carbons	25
2.2.3 Characterization.....	26
2.2.4 Electrochemical Measurements.....	26
2.3 Results and Discussion.....	27
2.3.1 Synthesis of Nitrogen Doped Carbons	27
2.3.2 Structural Analysis of Nitrogen Doped Carbon	29
2.3.3 Chemical Composition of Nitrogen Doped Carbons.....	35
2.3.4 Supercapacitor performance of N doped carbons.....	40
2.3.5 Effects of Iodine Pretreatment.....	45
2.4 Conclusions	48

REFERENCES	49
3.ACTIVATION OF NITROGEN DOPED CARBONS FOR SUPERCAPACITOR ELECTRODE MATERIAL	52
3.1 Introduction	52
3.2 Experimental Section.....	55
3.2.1 Activation Procedure of Nitrogen Doped Carbons.....	55
3.2.3 Characterization.....	55
3.2.4 Electrochemical Measurements.....	56
3.3 Results and Discussion.....	56
3.3.1 Activation Conditions of Nitrogen Doped Carbons	56
3.3.2 Structural Analysis of Activated Nitrogen Doped Carbon	59
3.3.3 Chemical Composition of Nitrogen Doped Carbons.....	63
3.3.4 Supercapacitor Performance of Nitrogen Doped Carbons	68
3.4 Conclusions	72
REFERENCES	73

LIST OF FIGURES

1.1: Performance of electrical capacitors, different types of batteries and conventional capacitors [2]	3
1.2: Schematic illustration of supercapacitors	4
1.3: Common types of nitrogen functionalities investigated in nitrogen-doped materials. [16]	9
1.4: Schematic outlining the general steps involved in the synthesis of hierarchical mesoporous carbons [54]	15
2.1: Schematic of the ice-templating synthesis procedure to produce N-doped porous carbon. ...	29
2.2: SEM images of C0.5-800. The SEM images reveal a fishbone like structure in the carbonized HPC material (a) with HR-SEM images showing the macroporous walls of this material (b).	30
2.3: EDS images for sample C0.5-800 (a); nitrogen (b) and carbon (c) distribution. Images were taken 20 keV for 60 s.	31
2.4: Nitrogen adsorption-desorption isotherms (a, c) and BJH adsorption pore-size distributions (b, d) of nitrogen doped carbons synthesized with different cyanamide fraction and carbonized at 800 and 1000 °C, respectively.....	33
2.5: Raman Spectra of (a) the 800 series of samples and (b) comparison of C0.5-800 and C0.5-1000	35
2.6: XPS survey spectra of the 800 °C (a) and 1000 °C (b) carbon series	36
2.7: High-resolution N1s (a, b) and O1s (c, d) spectra, for the 800 °C and 1000 °C carbon series.	39
2.8: Supercapacitance behavior of nitrogen doped carbon measured in a three-electrode system using 6 mol L ⁻¹ KOH solution as electrolyte within the potential range: 0-0.9 V (vs. Ag/AgCl): (a)	

cyclic voltammetry curves at different scan rates for sample C0.5-800; (b) cyclic voltammetry curves at 2mV/s for samples C0.5-800, C0.5-1000 and C0-800; (c)galvanostatic charge–discharge curves at various current densities for C0.5-800; (d) galvanostatic charge–discharge curves at 0.5A/g for C0.5-800, C0.5-1000 and C0-800.	40
2.9: Specific capacitance at various current density of the 800 carbon series (a) and the 1000 carbon series (b); specific capacitance plotted against nitrogen content; (d) electrical conductivities of nitrogen doped carbons as a function of nitrogen content.	43
3.1: Schematic showing the four basic steps and material prepared after each step. The four steps shown clockwise from top left are: a (top view) ice templating - ice front movement through the sucrose, cyanamide and colloidal silica aqueous suspension forming ice crystals; b (top view) freeze drying - the surose-cyanamide-silica composite material with macropores after removal of ice;c (top view) carbonization and silica etching results in macro-mesopore dominated carbon; d Physical activation, to introduce micropores.[1]	53
3.2: Nitrogen adsorption-desorption isotherms and BJH adsorption pore-size distributions of C0.5-800 activated under different conditions.	58
3.3: Relationship between the yield and the nitrogen content in the pristine none-activated carbon	59
3.4: Nitrogen adsorption-desorption isotherms (a, b) and BJH adsorption pore-size distributions (c, d) of nitrogen doped carbons carbonized at 800 and 1000 °C before and after activation process, respectively.....	60
3.5: The Raman Spectra of the nitrogen doped carbon before and after activation	63
3.6: Nitrogen content in 800NA, 800A, 1000NA and 1000A carbon Series	64
3.7: High-resolution N1s (a, b) and O1s (c, d) spectra, for the activated samples.	67
3.8: Supercapacitance behavior of activated nitrogen doped carbon measured (a) cyclic voltammetry curves at different scan rates for sample 0.5-800A; (b) cyclic voltammetry curves at 2mV/s for sample 0.5-800A, 0.5-1000A and 0.5-800NA; (c) galvanostatic charge–discharge curves at various current densities for sample 0.5-800A; (d) galvanostatic charge–discharge curves at 0.5A/g for sample 0.5-800Aand 0.5-800NA.....	68

3.9: Specific capacitance at various current densities of the activated 800 carbon series (a) and the activated 1000 carbon series (b); specific capacitance plotted against nitrogen content; (d) electrical conductivities of nitrogen doped carbons as a function of nitrogen content..... **71**

3.10: (a) cycling stability measured for 0.5-800A in three-electrode set up; (b) charge-discharge curve of the first and 600th cycle for 0.5-800A..... **72**

LIST OF TABLES

1.1: Specific surface area and specific pore volumes of various carbons synthesized [54].....	16
2.1: Surface area and pore volume of nitrogen doped carbons.....	32
2.2: I_D/I_G Ratio for nitrogen doped carbon synthesized by carbonization at 800 and 1000 °C.....	34
2.3: Atomic Composition of Nitrogen-Doped Carbon Samples.....	35
2.4: Characterization of the different types of nitrogen and oxygen groups present	37
2.5: Specific Capacitance of All Nitrogen-Doped Carbons at Low Current Density.....	42
2.6: Chemical Composition and Capacitance of Samples With/Without Iodine Pretreatment.....	48
3.1: Specific surface area and yield of final carbons for different activation conditions.....	57
3.2: Surface area and pore volume of nitrogen doped carbons before and after activation.....	59
3.3: I_D/I_G Ratio for nitrogen doped carbon before and after activation.....	62
3.4: Atomic composition of samples before and after activation.....	65
3.5: Characterization of the different types of nitrogen and oxygen dopants.....	66

3.6: Specific capacitance of nitrogen-doped carbons before and after activation at low current density70

CHAPTER 1

INTRODUCTION

1.1 Introduction to Supercapacitors

From wood fuel to coal and fossil oil, carbon materials have continued to play a critical role in the energy field throughout human history. Since the end of World War II, the world population has increased dramatically, which led to the wide use of carbon-material-based energy. Unfortunately the use of carbon has led more and more to serious greenhouse effect. Moreover, fossil fuels such as coal, oil and natural gas are all non-renewable resources. The mass consumption of fossil fuels has resulted in energy crisis and this has influenced greatly the world ecology and economy. Nowadays, to solve this energy crisis, people are proposing to use the bountiful, renewable and clean energy like solar energy and wind energy. This clean energy, in principle, should be able to meet the ever increasing and urgent energy needs. Modern technology has reduced the cost of utilizing the wind, solar, hydropower and other alternative energies. However, most clean energy like solar and wind are unpredictable and intermittent, which makes energy conversion and storage technology also essential. In many application fields, batteries, fuel cells, electrochemical capacitors (electrochemical or supercapacitors) have been proved to be the most efficient and the most practical energy conversion and storage devices.

Supercapacitors are a new type of capacitor used to store electrical energy based on interface electric double layer proposed by the German physicist Helmholtz. Since Becker invented and patented the use of carbon black for polarized electrode in 1957, the technologies regarding supercapacitors have been growing. Especially in 1983, the Japanese company NEC realized the commercial value of supercapacitors and introduced them to the market, which propelled supercapacitors and related research to the forefront.

[1] In general, supercapacitors are a new type of energy storage device, which combines the advantages of both conventional dielectric capacitors and rechargeable batteries. The comparison of performance between electrical capacitors, different types of batteries and conventional capacitors can be seen in Figure 1.1 [2]. Supercapacitors can deliver high output power within a very short time and store high energy with long cycle life and environmental friendly characteristics. [3] This is why supercapacitors were listed as one of the seven most significant world science and technology discoveries in 2006 by the Discover magazine, which stated that supercapacitors were a revolutionary development in the field of energy storage, and will replace traditional batteries in many application fields. So far, supercapacitors are widely used in applications such as consumer electronics, internal storage backup systems, industrial power and energy management systems. [4]

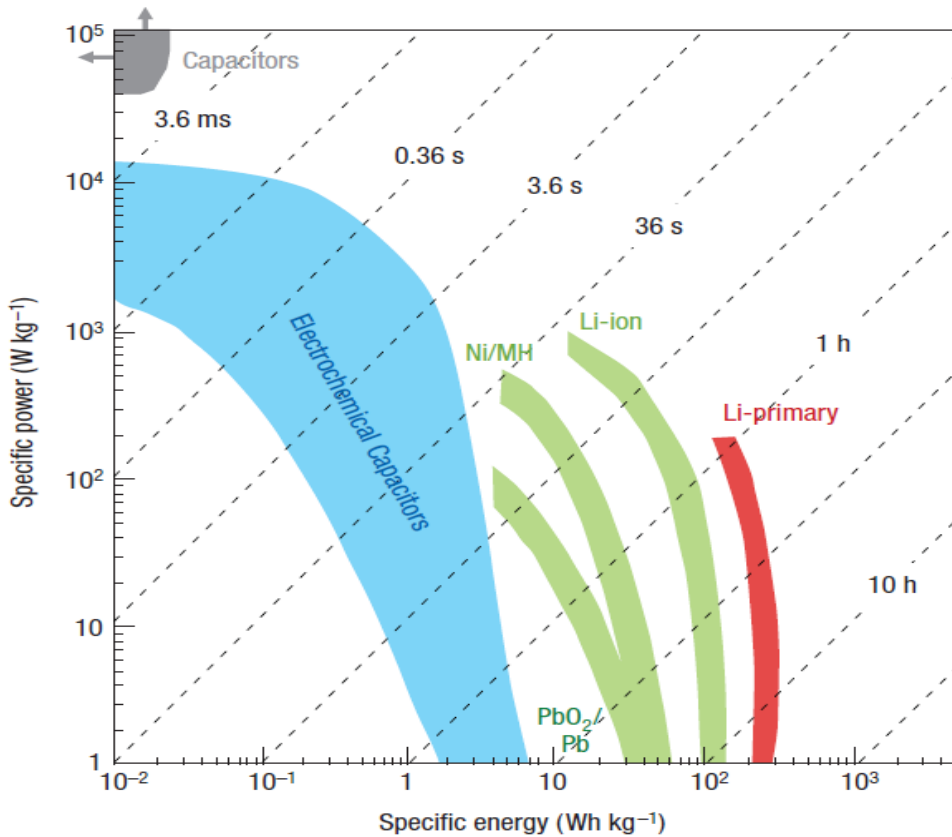


Figure 1.1: Performance of electrical capacitors, different types of batteries and conventional capacitors [2]

Supercapacitors are a device similar to a battery both in design and manufacture. As shown in Figure 1.2, it mainly consists of two electrodes, electrolyte, separator and current collector. [5] According to the working mechanism, supercapacitors can be divided into two types: electric double layer capacitors (EDLCs), the capacitance of which is generated basically from the electric double layer produced by the charge separation of the electrode/electrolyte interface (e.g. supercapacitors with carbon-based

electrodes, where there is no electrochemical reaction happening on the electrodes); the other one is called faradaic supercapacitor or pseudocapacitor (FSs) with electrochemical active electrode materials such as transition metal oxides (RuO_2 , MnO_2 , NiO) and conducting polymers (PANI and PPY). The capacitance of FSs is generated from underpotential deposition of electroactive ions onto the surface of metal oxide electrodes, or from the redox reaction happening on the metal oxide electrodes. [6-8]

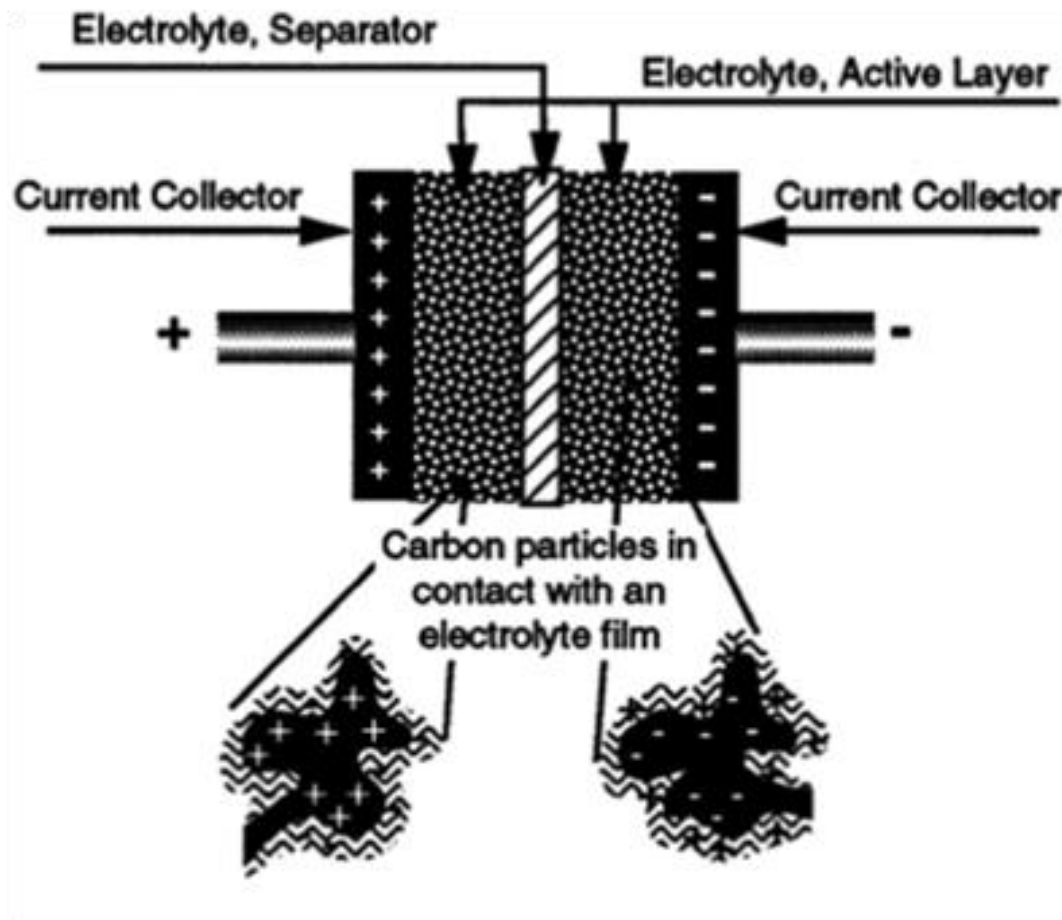


Figure 1.2: Schematic illustration of supercapacitors

For both electric double layer capacitors and faradaic supercapacitors, their performance mainly depend on their electrode materials, which is the most important part for supercapacitors. Ideal material for electrodes should possess large surface area, high

electrical conductivity, proper pore size, high mechanical strength, good electrochemical stability and good surface affinity toward the electrolyte. Among all the electrode materials, carbon materials have been generally the most studied option. [9, 10]

1.2 Introduction to Mesoporous Carbon

Carbon-based materials have distinct characteristics found in a variety of different forms and with various micro-textures. This makes carbon-based materials an ideal choice for applications ranging from catalysis to metal refining and fuel cells.[11] Highlighted by some of the top scientific awards, carbon-based materials such as carbon nanotubes, graphene and fullerenes have attracted broad scientific attention and have already been studied in depth. Meanwhile, research of mesoporous carbons, as another family of carbon-based materials, is also attracting a lot of attention with promising potential in several applications.

According to the definition of the International Union of Pure and Applied Chemistry (IUPAC), mesoporous carbon refers to carbon-based solid that is based on either ordered or disordered networks with a broad or narrow distribution of pores in the range between 2 and 50 nm.[12] In fact, mesoporous carbons have controllable and excellent properties distinguishing them from traditional carbon-based materials in the way that they not only retain the original properties of carbons but are also appealing because of simple synthesis approaches, adjustable specific surface area and porosity, and also their interfacial properties. [13] Especially regarding energy conversion and storage devices,

mesoporous carbons are even more attractive due to their high surface areas, easily obtainable porosity and good electrical conductivity in addition to low cost all of which make them excellent material for electrodes.

1.3 Functionalization of Mesoporous Carbon

In order to enhance the properties of mesoporous carbons for their utility in energy storage devices, much effort has been devoted to the modification of the surface and framework of these carbons. Among many possible choices of modification, functionalization can modify their electronic, surface and interfacial properties, thus further increasing utility of mesoporous carbons across a broad range of applications. The presence of some functional groups on the carbon surface or framework containing electron-donating or electron-withdrawing heteroatoms like B [14], N [15-18], O [19-20], P [21] or S[22], can provide mesoporous carbons with acid/base characteristics, which results in the Faradaic interactions between the ions from the electrolyte and functional groups, and, thereby increase their capacitance by the pseudo-capacitive effect. [23]

1.4 Nitrogen Doping of Carbons

Among those chemical elements mentioned above, nitrogen doping has long been the most promising method and thus the most studied option. Nitrogen became the most

popular choice for efficient and beneficial functionalization of mesoporous carbons mainly for the following specific reasons:

1. N resides next to C on the periodic table. By replacing one C with N in the carbon framework the total number of electrons in the entire system will be tailored one electron at a time.
2. N has an atomic radius similar to that of C and thus replacing one C with one N in the carbon network can avoid significant lattice mismatch.
3. N-doping can introduce an n-type electronic modification to the carbon structure, which is similar to typical semiconducting materials. This structure enables the potential utility of these C–N structures in various important nano-electronic applications.[24]
4. Nitrogen is abundant in nature with easy accessibility and low health risk.

According to recent study on nitrogen-doped carbons, this modification tunes the morphological, electrical and chemical properties of the functionalized carbon framework while keeping the beneficial properties of the carbon to be utilized. As for applications in energy storage devices, the doping of nitrogen in mesoporous carbons can enhance their capacitance while still maintaining the good rate capability of the carbons. It is found that the presence of electron-donating nitrogen can increase physical and chemical characteristics of carbon electrode materials, such as electrical conductivity, surface polarity and surface affinity toward aqueous electrolytes. [25–29]

1.5 Synthesis Methods of Nitrogen Doped Mesoporous Carbon

As nitrogen proved to be the most efficient and beneficial choice for modification of mesoporous carbons, much effort has been placed on the synthesis of nitrogen doped mesoporous carbon materials. To date, three strategies for preparation of nitrogen doped mesoporous carbon have already been developed. They include post-synthesis modification, hard templating and soft templating approaches.

1.5.1 Post-Synthesis Modification Methods

Post-synthesis modification of mesoporous carbon materials has been already investigated in depth. In a typical process, the pristine mesoporous carbons are treated with an organic nitrogen-containing precursor (most frequently ammonia) at high temperature to introduce nitrogen into the porous carbons frameworks [30]. Depending on the type of precursor, either aqueous or gaseous environments of treatment can be applied, and different precursors will result in distinct final surface chemistry and porosity of the obtained modified carbon. Porous carbon materials treated with ammonia at high temperatures proved to have enhanced porosity and incorporated functional surface groups such as $-\text{CN}$, $-\text{NH}_2$, pyridinic-N, pyrrolic-N, and graphitic nitrogen due to free radicals produced during the heating of ammonia. [31-34] Common structures of the multiple types of nitrogen functionalities investigated in the Nitrogen-doped materials are shown in Figure 1.3. The content and type of nitrogen species depend in large part on the

treatment temperature. The pyridinic (398.4 eV) and graphitic (401.2 eV) nitrogen become more dominant at high temperatures. [33] This result is similar with the outcome of ammonia heat treatment for other carbon structures such as carbon nanotube and graphene.

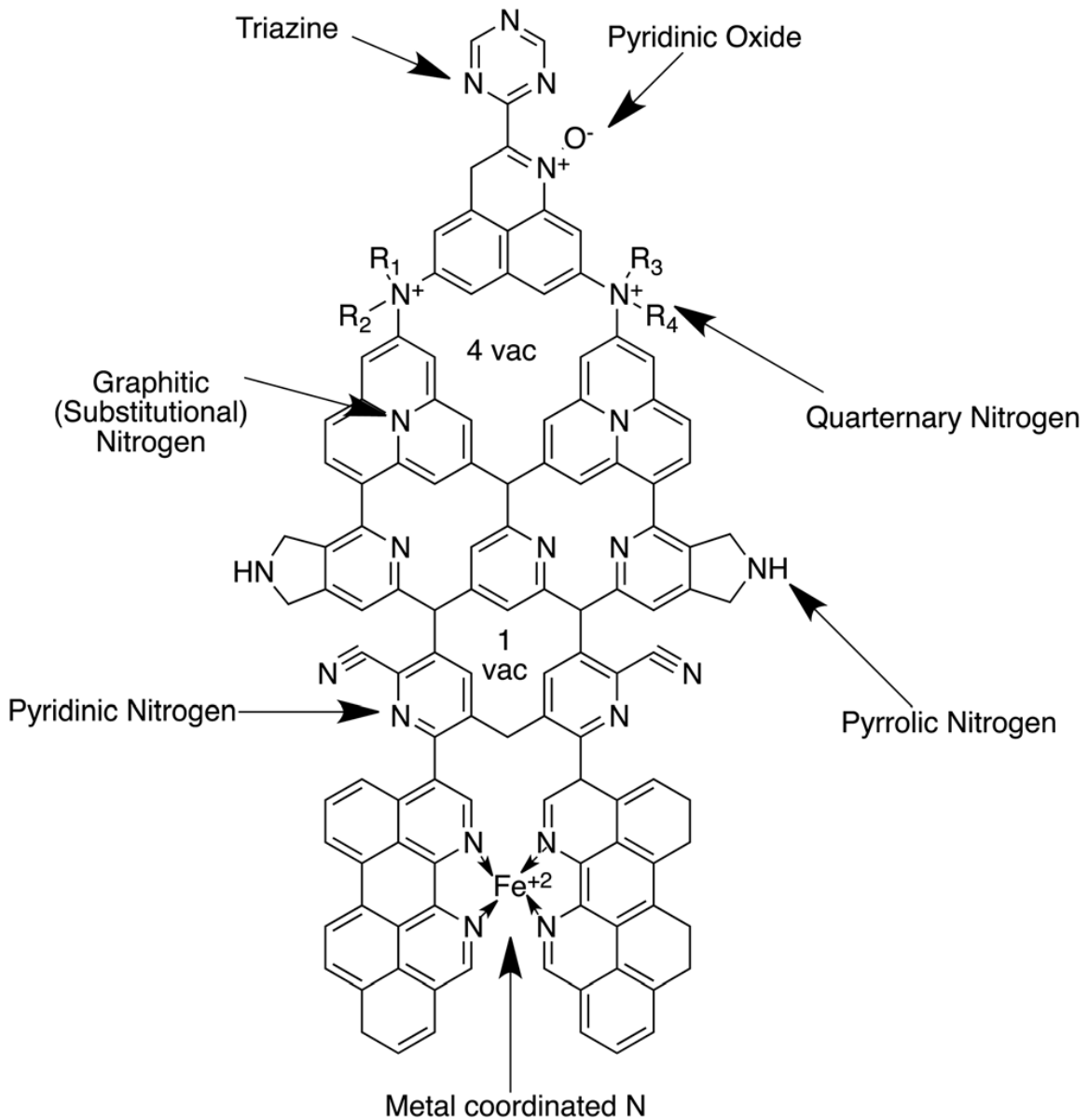


Figure.1.3: Common types of nitrogen functionalities investigated in nitrogen-doped materials. [16]

However, this post-synthesis modification method is not as tunable in either the amount or distribution of nitrogen dopants and can result in the collapse of pore structure of mesoporous carbon. [30] This treatment approach can only give nitrogen loading as high as 5% in the carbon matrix. Also, it is reported that nitrogen doped porous carbon materials synthesized through this post-synthetic amine modification process lack in stability and have an unsatisfactory performance for many applications.[34] As a result, recent efforts on nitrogen doped mesoporous carbons have been devoted to direct ‘one pot’ synthesis such as hard templating and soft templating approaches.

1.5.2 Hard Templating Methods

Hard templating or nanocasting strategy is a well-studied method of direct synthesis of nitrogen doped carbons, since it allows control of the morphology and pore structure of the final mesoporous carbons with incorporation of nitrogen into their networks simultaneously. [35] Usually ordered mesoporous silica such as SBA-15[23,36], MCM-48[37] and IBN-9[38] were chosen as a hard template, and a variety of organic N-containing compounds such as polymerized polyaniline (PAN)[37,39], p-diaminobenzene (DAB)[40], and cyanamide[23] could be used as a nitrogen dopant.

Shi et al. have demonstrated mesoporous nitrogen-doped carbons synthesized through carbonization in a silica SBA-15 using phenolic resin as a carbon source and high nitrogen-containing cyanamide as the nitrogen dopant. The obtained material had remarkably high nitrogen content up to 15 wt.%. Moreover, it is worth emphasizing the

incorporation of cyanamide not only introduced high nitrogen content into the carbon matrix mainly in forms of pyridinic and quaternary species, but also greatly enhanced the surface area of the final carbon materials. The final nitrogen-doped mesoporous carbon exhibited high surface area ($1741 \text{ m}^2/\text{g}$) and large pore volume ($1.2\text{--}1.81 \text{ cm}^3/\text{g}$). These improvements together with high nitrogen content led to a high specific capacitance (230 F/g at 0.5 A/g) and good rate capability.[23]

Zhao et al. pioneered a hard templating strategy focused on creating N-doped porous carbon nanostructures using tri-continuous mesoporous silica IBN-9. By rationally choosing carbon precursors and carefully controlling activation conditions they prepared an optimized porous carbon material which possessed a rather high nitrogen doping concentration ($\sim 13 \text{ wt. \%}$) and exhibited an excellent CO_2 adsorption performance over a wide range of CO_2 pressures.[39]

For hard-templating strategy, currently an extensive amount of work has been devoted to ionic liquids in combination with hard template structures to produce controlled, porous carbon materials. Ionic liquids are molten salts with melting temperatures generally below $100 \text{ }^\circ\text{C}$, which possess low vapor pressure, high electrical conductivity, and excellent thermal stability. [32, 40] Nitrogen-containing ionic liquids has shown promising potential as precursors for nitrogen-doped carbon materials because of the large amount of available anion and cation combinations, which allows better control over the species and extent of nitrogen doping. Moreover, their low vapor pressure enables the completion of carbonization process without evaporation. [41, 42] Wilson et al. demonstrated a way to synthesizing nitrogen doped porous carbons aimed to enhance

capacitive performance by combining a phenol-formaldehyde precursor with the ionic liquid (IL) 1-ethyl-3-methylimidazolium dicyanoamide (EMI-DCA) as the nitrogen dopant. The IL fraction in the precursor mixture affected the structural integrity, resistance and specific capacitance of the porous materials. When the IL fraction in the precursor was up to 50 wt. %, the electrode resistance was reduced while the bicontinuous mesoporous structure of the final carbon was preserved and the specific capacitance increased over 40% compared to mesoporous carbons synthesized using only the phenol formaldehyde resol. [43] Unfortunately, some reports indicated that the carbonization yield through these process could be low and also the cost of these materials could be high. [44]

1.5.3 Soft Templating Methods

The soft templating method is the simplest one among the three strategies. It is based on organic–organic assembly of the carbon precursor with amphiphilic surfactants such as phenolic resins, followed by template decomposition, and carbonization through heat treatment. Previous studies have found that the major challenge of the soft template approach is the limited options of suitable nitrogen-containing precursors. Proper precursors should be able to co-polymerize with phenolic resins to form ordered mesoporous structures and incorporate nitrogen in the carbon network during pyrolysis while simultaneously retain the mesoporous structures. [45-48] Yang et al. [49], Feng et al. [50] and Wei et al. [51] have illustrated successful examples of synthesizing nitrogen

doped mesoporous carbon through soft templating. They used dicyandiamid , urea and m-aminophenol as nitrogen source, respectively, with phenol–formaldehyde resol as carbon source. Especially, Wang et al. demonstrated direct pyrolysis of soft-templated polymeric composites in ammonia, which combined carbonization, functionalization, and activation into one simple process, creating large surface area ($\sim 1400\text{m}^2\text{ g}^{-1}$) nitrogen-doped (up to 9.3 at.% nitrogen) ordered mesoporous carbons [52] However, attempts to increase the proportion of N-containing precursors resulted in deterioration of the ordered mesoporous structures and therefore so far most of the obtained materials had nitrogen content less than 10 wt.%. Furthermore, the specific surface area of the N-doped mesoporous carbons was mostly less than $1500\text{m}^2/\text{g}$ because the poor thermal stability of nitrogen containing precursors caused serious shrinkage. [53] Therefore, developing an approach for direct synthesis of mesoporous carbon with high nitrogen content and also large surface area and high N-content is very desirable yet challenging.

1.6 Previous Work on Mesoporous Carbon in Our Group

Our group reported a novel synthesis approach of mesoporous carbons via an ice-templating method which is essentially a hard templating technique. [54] The obtained hierarchical porous carbons possess very high surface areas and large pore volumes (up to $2096\text{ m}^2\text{ g}^{-1}$ and $11.4\text{ cm}^3\text{ g}^{-1}$, respectively). It is an inexpensive and scalable method for making bulk quantities of carbon. Besides, the size of template can be varied which allows us to make carbons with highly tunable micro/meso/macro porosities.

The process can be divided into the following steps: a) making solution of glucose (carbon source) and commercially available stable suspensions of silica nanoparticles (hard template) in water. b) ice templating the solution by plunging in liquid nitrogen, followed by freeze drying which involves sublimation of the ice while the sample is kept under very low pressures. The purpose of ice templation is to introduce macroporosity of the order of few microns in the sample. This is because as the sample freezes in liquid nitrogen ice crystals grow phase separating the ice from silica and glucose, which after freeze drying form the walls of the macroporous structure. c) once dried completely, these samples are carbonized to convert the glucose into conducting carbon in an inert argon atmosphere inside a flow-through tube furnace. d) After carbonization, the silica nanoparticles are etched away to give rise to the pores in the walls of the network by using concentrated sodium hydroxide. e) After that, the specific surface area and extent of microporosity of the final carbon material can be further increased by CO₂ activation. Figure 1.6 shows a schematic of the entire synthesis route.

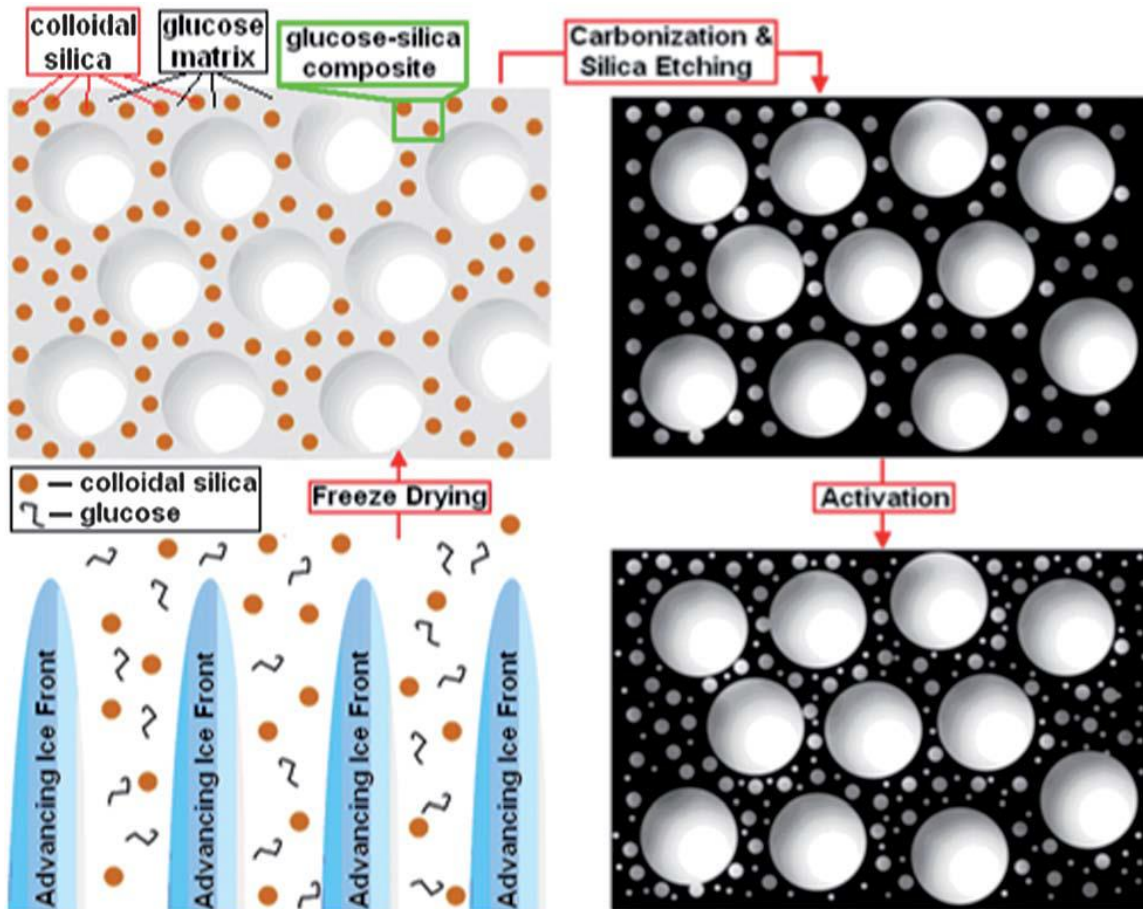


Figure 1.4: Schematic outlining the general steps involved in the synthesis of hierarchical mesoporous carbons [54]

Table 1.1 shows the surface area and pore volume for different carbons synthesized by the abovementioned technique. In general, the KCU-C x-2 samples showed the highest values for pore volumes among mesoporous carbon materials.[55] These carbon materials also showed good supercapacitors performance as the presence of mesopores and macropores can provide pathways for fast ionic transport and the micropores provide specific sites for ion adsorption.[56,57] The KCU 4-1-4 sample was tested in a three-

electrode setup and a specific capacitance of 221 F g⁻¹ was obtained at a scan rate of 2mV s⁻¹, with 64% preservation of capacity even at a scan rate of 200 mV s⁻¹. [54]

Table 1.1: Specific surface area and specific pore volumes of various carbons synthesized [54]

Sample name	BET surface area (m² g⁻¹)	N₂ adsorption pore volume (cm³ g⁻¹)
KCU-C 4-1-4	2096	3.0
KCU-C 4-1	1316	2.3
KCU-C 4-2	1327	4.1
KCU-C 8-1	1129	2.0
KCU-C 8-2	1265	3.6
KCU-C 12-1	893	1.9
KCU-C 12-2	1216	3.0
KCU-C 20-1	841	1.9
KCU-C 20-2	1289	3.7

In conclusion the ice-templating approach offers the following advantages:

1. The synthesis strategy enables easy control over the porosity. The extent of mesoporosity and the distribution of the mesopores can be tuned simply by either changing the weight ratio of silica to carbon precursor or using different size of silica. Additionally, as has been reported already in the literature, macropore structure and size can be tuned by manipulating the freezing rate of the precursor mixture into liquid nitrogen, by changing the concentration of carbon precursor,

- concentration and size of colloidal silica nanoparticle. [58, 59] Moreover, the reaction conditions of activation can control the microporosity.
2. This synthesis strategy is simple, repeatable, and uses low-cost and easy accessible reagents, which makes it a good option for making bulk quantities of carbon.

REFERENCES

- [1] B.E Conway, W.G Pell, *J. Solid State Electrochem*, **7**:637-644 (2003).
- [2] P. Simon, Y. Gogotsi, *Nature Materials*, **7**: 845-854 (2008).
- [3] C. Largeot, C. Portet, J. Chmiola, P. Taberna, Y. Gogotsi and P. Simon, *J. Am. Chem. Soc.* **130**: 2730 (2008)
- [4] G. P. Wang, L. Zhang, J. J. Zhang, *Chem. Soc. Rev*, **41**:797–8289 (2012).
- [5] R. Kotz and M. Carlen, *Electrochim. Acta*, **45**:2483 (2000).
- [6] B. E. Conway, *Electrochemical Supercapacitors*, Kluwer Academic/Plenum Press, New York (1999).
- [7] B. Babakhani and D. G. Ivey, *Electrochim. Acta*, **55**: 4014 (2010).
- [8] S. Sarangapani, B. V. Tilak and C. P. Chen, *J. Electrochem. Soc.*, **143**: 3791 (1996).

- [9] A. G. Pandolfo and A. F. hollenkamp, *J. Power Sources*, **157**: 11–27 (2006).
- [10] D. S. Su and R. Schlogl, *ChemSusChem*, **3**: 136–168 (2010).
- [11] P. Trogadas, T. F. Fuller, P. Strasser, *Carbon*, **75**: 5–42 (2014).
- [12] J. Rouquerol, D. Avnir, C. Fairbridge, D. Everett, J. Haynes, N. Pernicone, J. Ramsay, K. Sing and K. Unger, *Pure Appl. Chem*, **66**:1739–1758 (1994) .
- [13] X. Wang and Y. Song, *RSC Adv.*, **5**: 83239 (2015)
- [14] T. Wang, CX. Zhang, X. Sun, YX. Guo, H. Guo, J.Tang, *J Power Sources*, **212**:1–12 (2012).
- [15] J. Kim, M. Choi and R. Ryoo. *Bull. Korean Chem. Soc.*, **29(2)**:413-6 (2008).
- [16] W. Kim, MY. Kang, JB. Joo, ND. Kim, IK. Song, P. Kim, *J. Power Sources* **195(7)**:2125–9 (2010).
- [17] S. Shrestha and WE. Mustain, *J. Electrochem. Soc.*, **157 (11)**:B1665–72 (2010).
- [18] DW. Wang, F.Li, LC. Yin, X. Lu, Z-G. Chen, IR. Gentle, *Chem Eur J.* , **18(17)**:5345–51 (2012).
- [19] L. Zhao, LZ. Fan, MQ. Zhou, H. Guan, H. Qiao and M. Antonietti, *Adv. Mater.* ,**22(45)**:5202–6 (2010).
- [20] E. Raymundo-Pinero, F.Leroux and F. Beguin, *Adv. Mater.* , **18(14)**:1877–82(2006).
- [21] X. Zhao, Q. Zhang, B. Zhang, CM. Chen, A.Wang and T.Zhang, *J. Mater. Chem.*, **22(11)**:4963–9 (2012).

- [22] HK. Jeong, M. Jin, EJ. Ra, KY. Sheem, GH. Han and S. Arepalli, *ACS Nano* **4(2)**:1162–6 (2010).
- [23] Q. Shi, R. Zhang, Y. Lv, Y. Deng, A.A. Elzatahrya, and D. Zhao., *Carbon*, **84**:335-346 (2015).
- [24] K.N. Wood, R. O'Hayre and S. Pylypenko, *Energy Environ. Sci.*, **7**: 1212-1249 (2014).
- [25] V.V. Strelko, VS. Kuts and PA. Thrower, *Carbon*, **38(10)**:1499–503 (2000).
- [26] F. Su, CK. Poh, JS. Chen, G. Xu, D. Wang and Q. Li, *Energy Environ. Sci.*, **4(3)**:717–24 (2011).
- [27] M. Seredych, D. Hulicova-Jurcakova, GQ.Lu and TJ. Bandosz, *Carbon*, **46(11)**:1475–88 (2008).
- [28] D. Hulicova, J. Yamashita, Y. Soneda, H. Hatori, M. Kodama, *Chem. Mater.*, **17(5)**:1241–7 (2005).
- [29] E. Frackowiak, G. Lota, J. Machnikowski, C. Vix-Guterl and F. Beguin, *Electrochim. Acta.* , **51(11)**:2209–14 (2006).
- [30] Z. Wu, PA. Webley and D. Zhao, *J. Mater. Chem.*, **22(22)**:11379–89 (2012).
- [31] M. S. Shafeeyan, W. M. A. W. Daud, A. Houshmand and A. Shamiri, *J. Anal. Appl. Pyrolysis*, **89**:143–151 (2010).
- [32] W. Shen and W. Fan, *J. Mater. Chem. A*, **1**, 999 (2013).

- [33] D. Hulicova-Jurcakova, M. Kodama, S. Shiraishi, H. Hatori, Z. H. Zhu and G. Q. Lu, *Adv. Funct. Mater.* , **19**: 1800–1809 (2009).
- [34] S. Giraudet, Z. Zhu, X. Yao and G. Lu, *J. Phys. Chem. C*, **114**:8639–8645 (2010).
- [35] Y. Xia and R. Mokaya, *Adv. Mater.*, **16(17)**:1553–8 (2014).
- [36] R. Silva, D. Voiry, M. Chhowalla and T. Asefa, *J. Am. Chem. Soc.*, **135**: 7823–7826 (2013).
- [37] R. Ryoo, S. H. Joo and S. Jun, *J. Phys. Chem. B*, **103**: 7743 (1999).
- [38] YF. Zhao, L. Zhao, KX. Yao, Y. Yang, Q. Zhang and Y. Han, *J. Mater. Chem.*, **22**: 19726 (2012).
- [39] G. Liu, XG. Li, P. Ganesan and B. N. Popov, *Applied Catalysis B: Environmental*, **93**:156–165(2009).
- [40] J. P. Paraknowitsch, A. Thomas and M. Antonietti, *J. Mater. Chem.*, **20**: 6746 (2010).
- [41] Y.S. Li, I.W. Sun, J.-K. Chang, C.-J. Su and M.T. Lee, *J. Mater. Chem.*, **22**: 6274-6279 (2012).
- [42] B. Qiu, C. Pan, W. Qian, Y. Peng, L. Qiu, F. Yan, *J. Mater. Chem. A*, **1**: 6373-6378 (2013).
- [43] B. E. Wilson, SY. He , K. Buffington , S. Rudisill ,W.H. Smyrl, A. Stein , *J. Power Sources*, **298**:193-202 (2015).

- [44] J. S. Lee, X. Wang, H. Luo, G. a. Baker and S. Dai, *J. Am. Chem. Soc.*, **131**: 4596–4597 (2009).
- [45] C. D. Liang, K. L. Hong, G. A. Guiochon, J. W. Mays and S. Dai, *Angew. Chem., Int. Ed.*, **43**: 5785 (2004).
- [46] C. D. Liang and S. Dai, *J. Am. Chem. Soc.*, **128**: 5316 (2006).
- [47] F. Q. Zhang, Y. Meng, D. Gu, Y. Yan, C. Z. Yu, B. Tu and D. Y. Zhao, *J. Am. Chem. Soc.*, **127**: 13508 (2005).
- [48] Y. Meng, D. Gu, F. Q. Zhang, Y. F. Shi, H. F. Yang, Z. Li, C. Z. Yu, B. Tu and D. Y. Zhao, *Angew. Chem., Int. Ed.*, **44**: 7053 (2005).
- [49] J. P. Yang, Y. P. Zhai, Y. H. Deng, D. Gu, Q. Li, Q. L. Wu, Y. Huang, B. Tu and D. Y. Zhao, *J. Colloid Interface Sci.*, **342**: 579 (2010).
- [50] C. M. Feng, H. X. Li and Y. Wan, *J. Nanosci. Nanotechnol.*, **9**:1558 (2009).
- [51] J. Wei, D. Zhou, Z. Sun, Y. Deng, Y. Xia, D. Zhao, *Adv. Funct. Mater.*, **23** (18):2322–8 (2013).
- [52] XQ. Wang, C-G. Liu, D. Neff, P. F. Fulvio, R. T. Mayes, A. Zhamu, Q. Fang, GR. Chen, H. M. Meyer, B.Z. Jang and S. Dai *J. Mater. Chem. A*, **1**:7920 (2013)
- [53] O. Barbieri, M. Hahn, A. Herzog, R. Kotz, *Carbon*, **43**(6):1303–10 (2005).
- [54] L. Estevez, R. Dua, N. Bhandari, A. Ramanujapuram, P. Wang and E. P. Giannelis. *Energy Environ. Sci.*, **6**: 1785 (2013).

- [55] A. H. Lu, W. Schmidt, B. Spliethoff, and F. Schuth, *Adv. Mater.* , **15**:1602–1606 (2003).
- [56] F. Xu, R. Cai, Q. Zeng, C. Zou, D. Wu, F. Li, X. Lu, Y. Liang and R. Fu, *J. Mater. Chem.*, **21**:1970–1976 (2011).
- [57] Z. Chen, J. Wen, C. Yan, L. Rice, H. Sohn, M. Shen, M. Cai, B. Dunn and Y. Lu, *Adv. Energy Mater.*, **1**: 551–556 (2011).
- [58] M. C. Gutierrez, Z. Y. Garcia-Carvajal, M. Jobbagy, F. Rubio, L. Yuste, F. Rojo, M. L. Ferrer and F. del Monte, *Adv. Funct. Mater.* , **17**: 3505–3513 (2007)
- [59] S. Deville, C. Viazzi and C. Guizard, *Langmuir*, **28**:14892–14898 (2012).

CHAPTER 2

DESIGN AND SYNTHESIS OF MESOPOROUS CARBONS WITH TUNABLE AMOUNT OF NITROGEN DOPING

2.1 Introduction

In this chapter, we present synthesis of nitrogen doped mesoporous carbons possessing large surface area with high and tunable (~ 2-22 at.%) nitrogen doping levels via a hard templating strategy inspired by the ice-templating approach of hierarchical porous carbons previously reported by our group. [1] In this method, we use colloidal silica as the hard template for mesopores, sucrose as the primary carbon precursor and cyanamide as the nitrogen dopant and secondary carbon precursor. In addition, by using iodine/air stabilization pretreatment the nitrogen content can be increased. Parameters that were controlled during synthesis include the sucrose to cyanamide weight ratio, carbonization temperature, and the presence/absence of the iodine/air stabilization treatment steps.

Cyanamide possesses a very high nitrogen content of 66.7 wt. % and is mainly used to prepare graphitic carbon nitride (C_3N_4) by heating it up to 550 °C during which a polycondensation reaction happens. [2] Heating cyanamide further to above 600 °C will result in pyrolysis of cyanamide, during which a variety of active nitrogen species such as ammonia and cyano fragments can be gradually released, which can lead to in-situ formation of carbon network with high nitrogen content. [3, 4] A mesoporous carbon

network can be synthesized using an aqueous solution of, cyanamide and sucrose and silica as the hard template.

As many studies have reported previously, the stabilization environment has a significant influence on the yield and structure of the carbon material synthesized from organic precursors. Therefore, in our work additional iodine pretreatment together with air stabilization were employed to retain and stabilize cyanamide in the framework along with sucrose. Iodine pretreatment is a stabilization strategy, which is performed under iodine vapors and can increase the carbon yield of organic precursors such as pitch-model compounds that typically give very low yields, if pyrolyzed directly [5]. Air stabilization is also a widely used pretreatment procedure for various organic precursors. It is performed in air at a relatively low temperature (200 °C in this work) in order to thermally stabilize the structure by an oxidative stabilization mechanism that makes it infusible. [6]

2.2 Experimental Section

2.2.1 Materials

Colloidal silica (4 nm, 15wt. %), sucrose, sodium hydroxide was purchased from Alfa Aesar. Cyanamide (50 wt. % in water) was purchased from Sigma Aldrich, and Iodine crystals from Mallinckrodt Chemicals. All chemicals were used as received without further purification.

2.2.2 Synthesis Procedure of Nitrogen Doped Carbons

The nitrogen-doped carbons were prepared through a modified ice-templating synthesis route reported earlier by our group for the synthesis of hierarchical porous carbons [1]. For a typical synthesis, sucrose (carbon source) and cyanamide (nitrogen source) were dissolved in the colloidal silica suspension in water (15 wt. %) so that the final weight ratios of silica: sucrose: cyanamide were: 1:1:0.1, 1:1:0.2, 1:1: 0.3, 1:1:0.5 and 1:1:1. Then, the precursor mixture was dipped into liquid nitrogen until it is completely solidified during which phase separation of solids and ice crystals occurs. After this step, the precursor mixture was immediately transferred to a freeze dryer to sublime off the ice for over 2 days. Before carbonization a pretreatment involving two steps can be applied. First, the white material after freeze-drying was mixed with iodine crystal and heated together at 90 °C for 24 h in a closed tinted glass bottle placed in an oven, where the iodine vaporizes and reacts with the sucrose-cyanamide-silica mixture. Second, this brown-colored mixture was transferred into a crucible and heated for 4h at 200 °C inside an oven. The color of the mixture turns black after this pretreatment. For the carbonization step, the mixture was maintained at either 800 °C or 1000 °C for 3 h under argon at a heating rate of 3 °C min⁻¹. After carbonization, a solution of 3M sodium hydroxide was used and the obtained carbon was stirred in this solution at 80 °C overnight during which time the silica got completely dissolved and removed. After that, the remaining material was repeatedly rinsed with deionized water till pH 7. The final carbon samples were then dried in a vacuum oven under at 80 °C for about 2 days to remove any remaining water from the sample.

2.2.3 Characterization

The morphology and microstructures of samples were imaged by Scanning Electron Microscopy (SEM) and Energy Dispersive X-Ray Spectroscopy (EDS) using a LEO 1550 FESEM operating between 2-20 keV. SEM samples were prepared using a cryo-microtome (Leica EM FC7). Raman spectra were recorded with a Renishaw InVia Confocal Raman microscope. Nitrogen sorption isotherms were obtained at 77K using Micromeritics ASAP 2460 analyzer. The Brunauer-Emmett-Teller (BET) model was applied to calculate the specific surface area and Barrett-Joyner-Halenda (BJH) model was used to obtain pore size distributions and total pore volume from the adsorption branch of isotherms. The chemical composition and bonding information of C, N and O was analyzed by X-ray photoelectron spectroscopy (XPS) using a Surface Science Instruments SSX-100 operating pressure of $\sim 1 \times 10^{-8}$ Torr.

2.2.4 Electrochemical Measurements

All nitrogen doped carbons were tested as electrochemical supercapacitors and all electrochemical experiments were carried out on a Solartron electrochemical workstation in a three-electrode system at room temperature. To prepare the electrodes, a thick slurry consisting of 80 wt % obtained carbon material, 10 wt % carbon black (SuperP), and 10 wt % polyvinylidene fluoride (PVDF) as binder, respectively, using N-

methylpyrrolidone (NMP) as the solvent was mixed uniformly, pressed onto a nickel foam (current collector) and dried at 80°C in oven. The mass of nitrogen doped carbon on each nickel foam was around 3.0~6.0 mg in an area around 1.0 cm². In a three-electrode set up, platinum wire was used as the counter electrode, Ag/AgCl as the reference electrode, and sample carbon coated nickel foam as the working electrode with 6 M KOH aqueous solution as the electrolyte. Cyclic voltammetry (CV) curves were carried out within the potential range of 0-0.9 V vs Ag/AgCl by varying the scan rate from 2 to 50 mVs⁻¹. Charge-discharge measurements were tested galvanostatically at 0.5-25A g⁻¹ within a voltage range of 0-0.9 V vs Ag/AgCl.

2.3 Results and Discussion

2.3.1 Synthesis of Nitrogen Doped Carbons

The synthetic strategy used in this work is demonstrated in Figure 2.1. This method is an adaptation with several modifications of a previously reported approach by our group to synthesize hierarchical porous carbons through ice templating. Cyanamide has high nitrogen content but is not a good carbon precursor because its low temperature polymerization product carbon nitride decomposes at high carbonization temperatures (beyond 600 °C) [7]. That is why cyanamide was added along with sucrose as the primary carbon source, which is an excellent carbon precursor. For a typical synthesis using ice templating, first, suspensions of sucrose, cyanamide and colloidal silica in water

were prepared. Since both sucrose and cyanamide are soluble in water, they distribute uniformly around the silica nanoparticles at the molecular level. Then, the suspensions were immersed into liquid nitrogen during which nucleation and growth of ice crystals separate the solids and lock in the structure with sucrose, cyanamide and silica forming walls around the ice crystals. This mixture is then transferred to a freeze dryer immediately, where ice sublimates without melting the structure, avoiding any aggregation or rearrangement of the silica nanoparticles, which is important for obtaining sharp mesopore size distributions in the final carbon. Iodine pretreatment can be employed before the carbonization step and it has been proved to be effective in thermally stabilizing the polymeric precursors during carbonization by cyclization, ring fusion or chain cross-linking of precursors before carbonization [8]. By varying the weight ratios of sucrose and cyanamide in the initial suspensions, adjusting the carbonization temperature (800 °C and 1000 °C), and by applying the iodine and air stabilization pretreatment, a series of nitrogen-doped carbons with tunable nitrogen content was synthesized. The notation of samples is as follows: C_x-y-z, where x is the mass ratio of cyanamide/sucrose, y is the carbonization temperature, and z whether I₂/air treatment was used (as applicable).

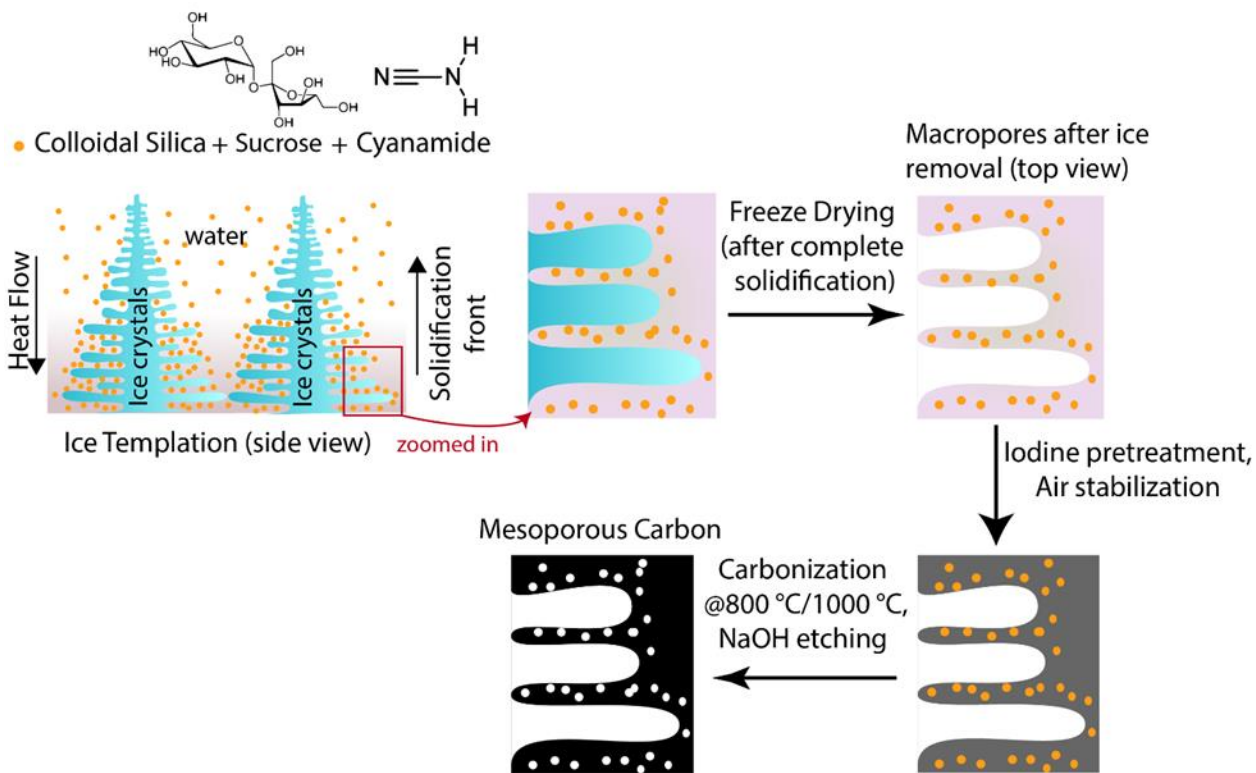


Figure 2.1: Schematic of the ice-templating synthesis procedure to produce N-doped porous carbon.

2.3.2 Structural Analysis of Nitrogen Doped Carbon

For supercapacitor performance, the mesoporosity and microporosity are of great significance and therefore, an interconnected macroporous framework that would enable easy access to the higher surface area and meso-, micropores is also of importance. In order to determine the morphology and size of the ice templated macroporous structure, Scanning Electron Microscopy (SEM) together with Energy Dispersive X-Ray

Spectroscopy (EDS) were used. Figure 2.2 and Figure 2.3 are the SEM and EDS images of the final nitrogen doped carbon sample 0.5-800. Figure 2.2.a shows the general fishbone-like structure of the ice-templating, which is prevalent after carbonization [9]. Figure 2.2.b shows the macroporous walls of this hierarchical porous carbon material. We also used Energy-dispersive X-ray spectroscopy (EDS) while imaging the sample. The elemental mapping image (Figure 2.3.a and b) confirmed that nitrogen was uniformly distributed into the carbon framework.

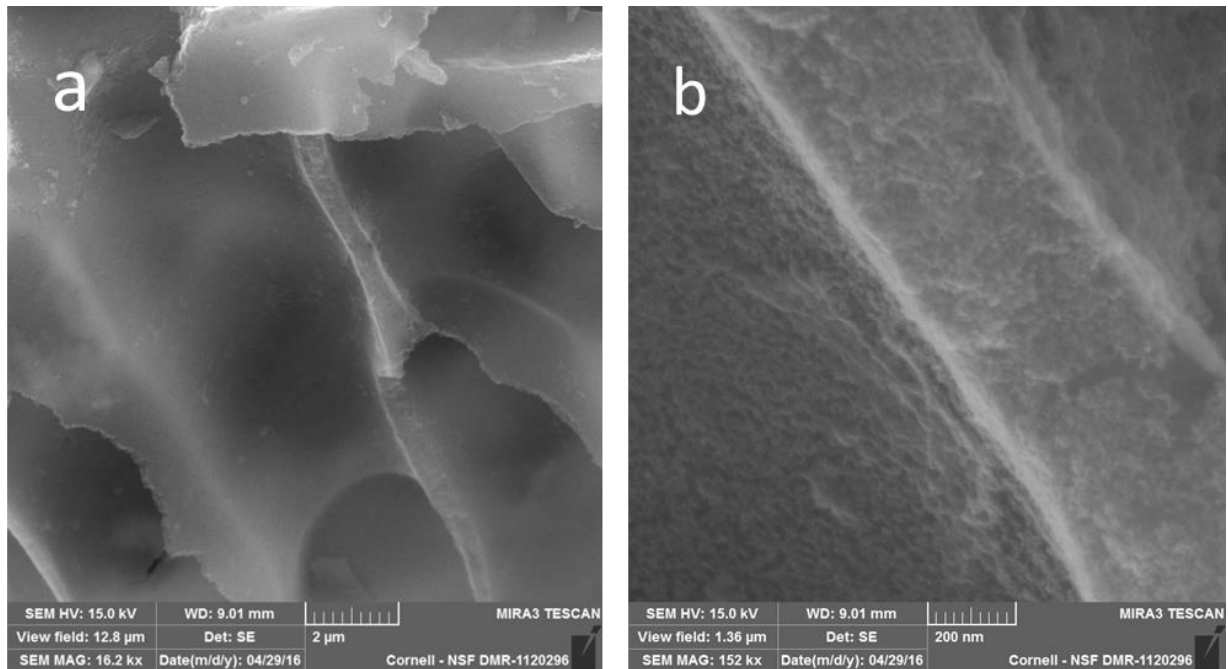


Figure 2.2: SEM images of C0.5-800. The SEM images reveal a fishbone like structure in the carbonized HPC material (a) with HR-SEM images showing the macroporous walls of this material (b).

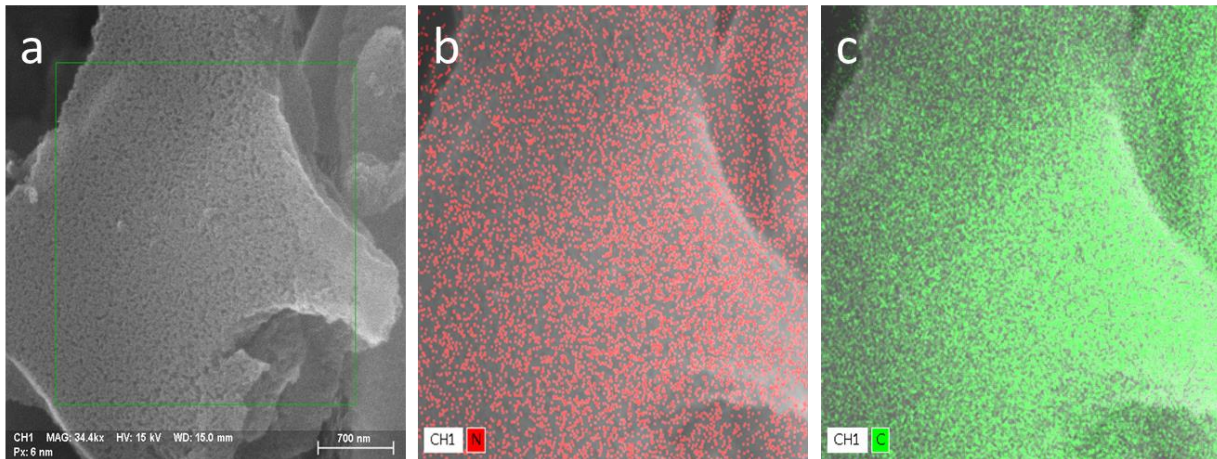


Figure 2.3: EDS images for sample C0.5-800 (a); nitrogen (b) and carbon (c)

distribution. Images were taken 20 keV for 60 s.

The specific surface area and pore volume of all the nitrogen doped carbon synthesized without iodine pretreatment were calculated using the Brunauer-Emmett-Teller (BET) model and Barrett-Joyner-Halenda (BJH) model from nitrogen adsorption/desorption isotherms and the results are shown in Table 2.1. In general, the specific surface area was high and the pore volume of mesopores was quite high among mesoporous carbon reported. The carbon material prepared through the same procedure but without cyanamide in the precursor mixture, C0-800, has specific surface area of $1023 \text{ m}^2/\text{g}$ and mesopore volume of $1.91 \text{ cm}^3/\text{g}$. As the cyanamide fraction in the precursor increased, the specific surface area and pore volume slightly decreased. However as cyanamide/sucrose weight ratio reached 1.0, it resulted in significance shrinkage in the final carbon framework and the specific surface area dropped to $\sim 770 \text{ m}^2/\text{g}$. Since the amount of sucrose per gram of silica is the same in all carbons, the results show that the cyanamide to sucrose weight ratio plays a crucial role in determining how effectively the resulting carbon replicates the colloidal silica network as cyanamide likely destroys the

pore structure to some extent. It is worth mentioning that enough amount of sucrose per gram of silica (1:1 in this study) must be used to retain the porosity. A lower ratio leads to collapse of mesoporous structure especially when the ratio of cyanamide to sucrose is high.

Table 2.1 Surface area and pore volume of nitrogen doped carbons

sample	BET surface area (m²/g)	V_{meso} (cm³ g⁻¹)	V_{micro} (cm³ g⁻¹)	sample	BET surface area (m²/g)	V_{meso} (cm³ g⁻¹)	V_{micro} (cm³ g⁻¹)
0.1-800	1028	2.06	0.023	0.1-1000	1009	2.27	0.030
0.2-800	1008	1.67	0.009	0.2-1000	996	1.96	0.012
0.3-800	979	1.39	0.004	0.3-1000	974	1.85	0.021
0.5-800	923	1.27	0.009	0.5-1000	975	1.58	0.012
1.0-800	765	1.02	0.042	1.0-1000	771	1.00	0.009

To visualize the nature of porosity and how it changes with the synthesis conditions, nitrogen adsorption-desorption isotherms and BJH pore size distributions are presented in Figure 2.4. All samples in figure 2.4.a and c show similar type IV isotherms with a clear capillary condensation step at around P/Po =0.5-0.7, which indicates the presence of mesoporous network in all obtained carbon materials. It is clear in Figure 2.4.a and c that the volume of nitrogen adsorbed decreases as the cyanamide/sucrose weight ratio increases, indicating a less developed mesoporosity. Pore size distribution curves as plotted in Figure 2.4b and d also reveal a sharper distribution of pore size centered at ~5-6 nm in agreement with the original silica nanoparticle size (4nm) for carbon samples

with lower cyanamide ratio. Moreover, according to Figure 2.4.d, compared to the 800 series, the 1000 samples had more macropores.

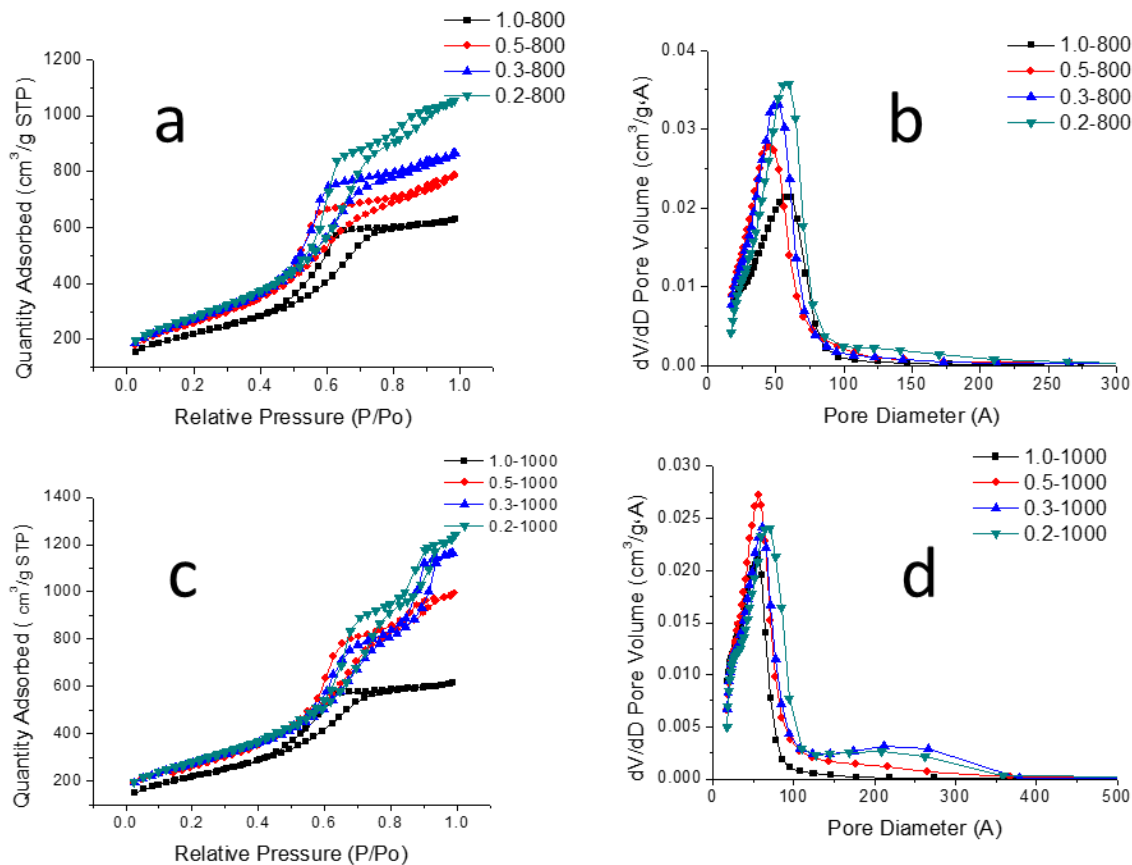


Figure 2.4: Nitrogen adsorption-desorption isotherms (a, c) and BJH adsorption pore-size distributions (b, d) of nitrogen doped carbons synthesized with different cyanamide fraction and carbonized at 800 and 1000 °C, respectively.

Raman spectroscopy is strongly sensitive to the electronic structure in the carbon material and thus it has been widely used to characterize carbon-based materials, especially for distinguishing carbon–heteroatoms bonds from carbon–carbon bonds and ordered and

disordered crystal structures. [10] The unique peaks of carbon-based materials in Raman spectra are the D band at $\sim 1350 \text{ cm}^{-1}$, which is related to disordered structures and the G band at $\sim 1580 \text{ cm}^{-1}$, which arises from the first-order scattering of the E_{2g} mode of sp^2 carbon domains. [11, 12] In figure 2.5.a. we showed the Raman spectra of the samples synthesized with different cyanamide fraction and carbonized at $800 \text{ }^\circ\text{C}$. As the cyanamide fraction increased from 0 to 1.0, the position of G-band shifted from 1594 cm^{-1} to 1544 cm^{-1} while the position of D-band shifted from 1351 cm^{-1} to 1374 cm^{-1} . The dependence of the position of the G-band and the D-band on the nitrogen content is obvious, probably related to the types of nitrogen dopant in the network. Additionally, the weak and broadened 2D peak showed that the obtained nitrogen doped carbon possessed some defects. Fig. 2.5.a and b also show that the intensity ratio of the D-band to the G-band (I_D/I_G) decreases with increasing carbonization temperature while increases with higher cyanamide fraction, suggesting that the lower carbonization temperature and higher cyanamide fraction leads to more defects in the carbon framework. The specific value of the I_D/I_G ratios are listed in Table 2.2

Table 2.2 I_D/I_G Ratio for nitrogen doped carbon synthesized by carbonization at 800 and $1000 \text{ }^\circ\text{C}$

sample	I_D/I_G	sample	I_D/I_G
0.3-800	1.2	0.3-1000	1.0
0.5-800	1.4	0.5-1000	1.2
1.0-800	1.4	1.0-1000	1.2

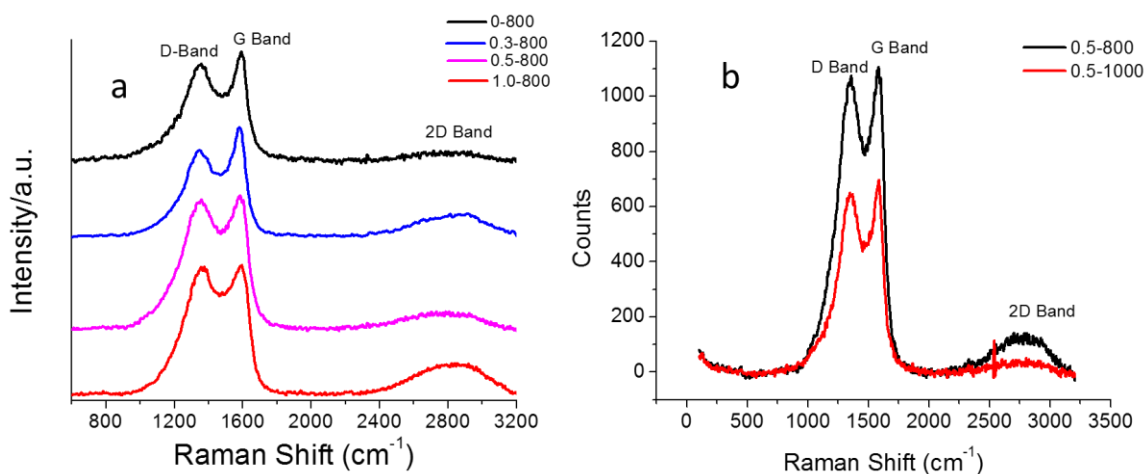


Figure 2.5: Raman Spectra of (a) the 800 series of samples and (b) comparison of C0.5-800 and C0.5-1000

2.3.3 Chemical Composition of Nitrogen Doped Carbons

Table 2.3 Atomic Composition of Nitrogen-Doped Carbon Samples

Sample	N a.t.%	C a.t.%	O a.t.%	Sample	N a.t.%	C a.t.%	O a.t.%
0.1-800	4.6	88.6	5.3	0.1-1000	2.0	92.9	4.2
0.2-800	7.4	80.0	8.2	0.2-1000	2.4	87.2	7.5
0.3-800	10.1	84.5	4.4	0.3-1000	3.5	89.6	5.2
0.5-800	13.4	80.4	4.5	0.5-1000	4.8	86.2	6.4
1.0-800	19.0	74.2	4.3	1.0-1000	6.7	82.0	8.5

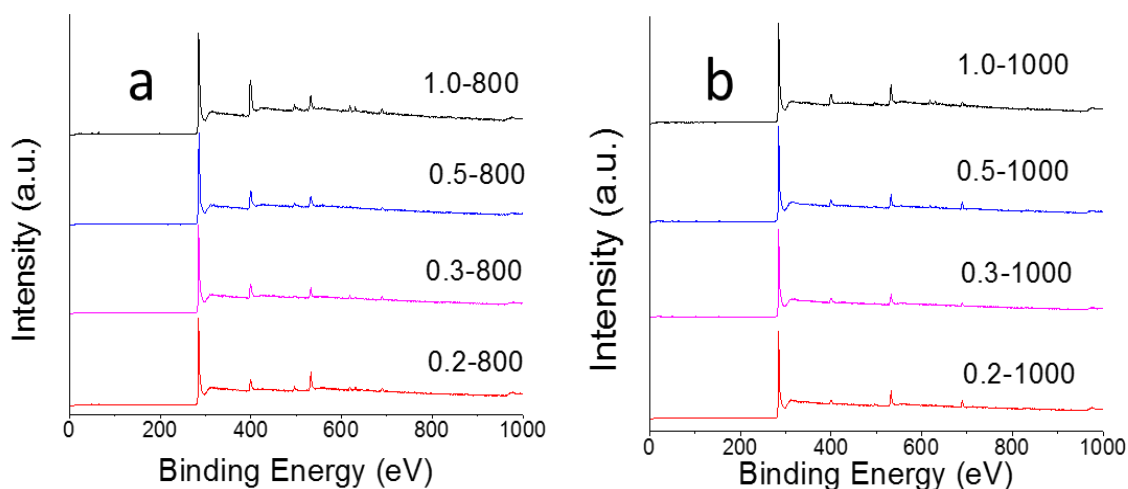


Figure 2.6: XPS survey spectra of the 800 °C (a) and 1000 °C (b) carbon series

X-ray photoelectron spectroscopy was used to determine the chemical compositions of all synthesized carbons samples. Figure 2.6.a and b show wide scan analysis which confirmed the presence of nitrogen along with significant amounts of oxygen. The exact atomic compositions calculated from these scans are listed in Table 2.3. In general, the nitrogen content of the samples at 800 °C was much higher than those pyrolyzed at 1000 °C, since nitrogen functional groups become unstable at higher temperatures. Also, as the cyanamide to sucrose weight ratio increased from 0.1 to 1.0 the nitrogen content increased dramatically. However, the oxygen content seemed to be independent of the carbonization temperature as well as the cyanamide fraction in the precursor.

The nature of nitrogen and oxygen dopants was further studied in detail from high-resolution spectra of the individual nitrogen (Figure 2.7.a and b) and oxygen 1s (Figure 2.7c and d) peaks observed in XPS analysis. The nitrogen N 1s peak could be deconvoluted into three nitrogen peaks centered at 398.4 eV, 400.4 eV and 403.6 eV corresponding to

pyridinic-N (N-6), pyrrolic/pyridone-N (N-5) and pyridine-N-oxide (N-X), respectively. N-5 and N-6 types were clearly the dominant nitrogen types in all carbons. These two types together account for over 80% of all nitrogen with their relative intensities varied from sample to sample. The exact ratio is listed in table 2.4. It is well known that only N-6 and N-5 are electrochemically active in alkaline electrolyte and, hence, responsible for the pseudocapacitive effect [13]. Similarly, oxygen O 1s peak was deconvoluted into three peaks centered at 531.6 eV, 533.0 eV and 535.8 eV for the 800 °C series, and, into 530.8 eV, 532.6 and 536.0 eV for the 1000 °C series of samples, respectively, with varying relative intensities. Unlike nitrogen, the predominant oxygen functional groups are different for carbons obtained at 800 °C and 1000 °C. For oxygen, the binding energies of 530.7 ± 0.1 , 531.4 ± 0.1 eV, 532.4 ± 0.1 eV, 533.7 ± 0.1 eV and 535 ± 0.1 eV are assigned to quinone type groups (O-1), C=O(O-2), C-O ether like(O-3), C-OH (O-4), and adsorbed water (O-5), respectively [14]. Therefore, for the 800 series, the dominant groups are C=O (O-1), C-OH (O-4). For the 1000 series the corresponding groups are quinone (O-1), C-O ether type (O-3). Among the various oxygen groups, only phenolic hydroxyl and carboxyl C=O are electrochemically active towards redox reactions in alkaline medium [15]. In summary, the types of both nitrogen and oxygen groups that exist in these carbons are favorable towards good supercapacitor performance for carbons carbonized at 800° C. However, for the 1000 series carbon, only the nitrogen groups present are favorable for pseudocapacitive reactions.

Table 2.4 Characterization of the different types of nitrogen and oxygen groups present

Sample	N-6	N-5	N-6/N-5	O-1	O-2	O-3	O-4	O-5
	%	%		%	%	%	%	%
0.1-800	23.0	62.0	0.37	-	29.3	-	34.7	27.5
0.2-800	35.5	53.7	0.66	-	14.2	-	77.5	8.3
0.3-800	26.0	54.9	0.47	-	18.0	-	73.3	8.7
0.5-800	24.4	75.4	0.32	-	38.4	-	45.1	16.5
1.0-800	20.9	77.7	0.27	-	35.7	-	60.9	3.3
0.1-1000	24.1	75.6	0.32	18.3	-	63.6	-	18.1
0.2-1000	27.8	53.6	0.52	24.2	-	66.9	-	8.9
0.3-1000	17.0	82.9	0.21	25.1	-	54.8	-	20.0
0.5-1000	26.9	56.4	0.48	12.1	-	51.0	-	29.8
1.0-1000	22.1	66.4	0.33	21.0	-	51.1	-	23.3

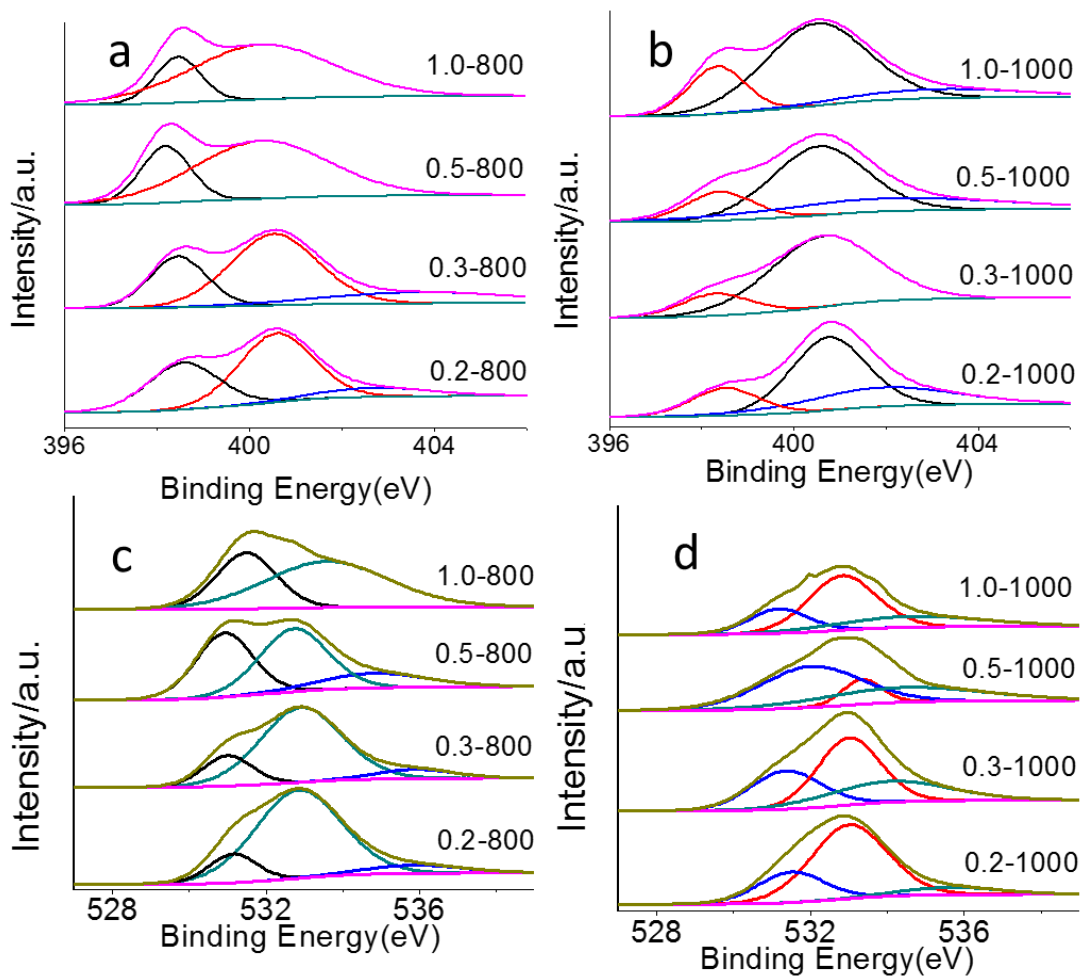


Figure 2.7: High-resolution N1s (a, b) and O1s (c, d) spectra, for the 800 °C and 1000 °C carbon series.

2.3.4 Supercapacitor performance of N doped carbons

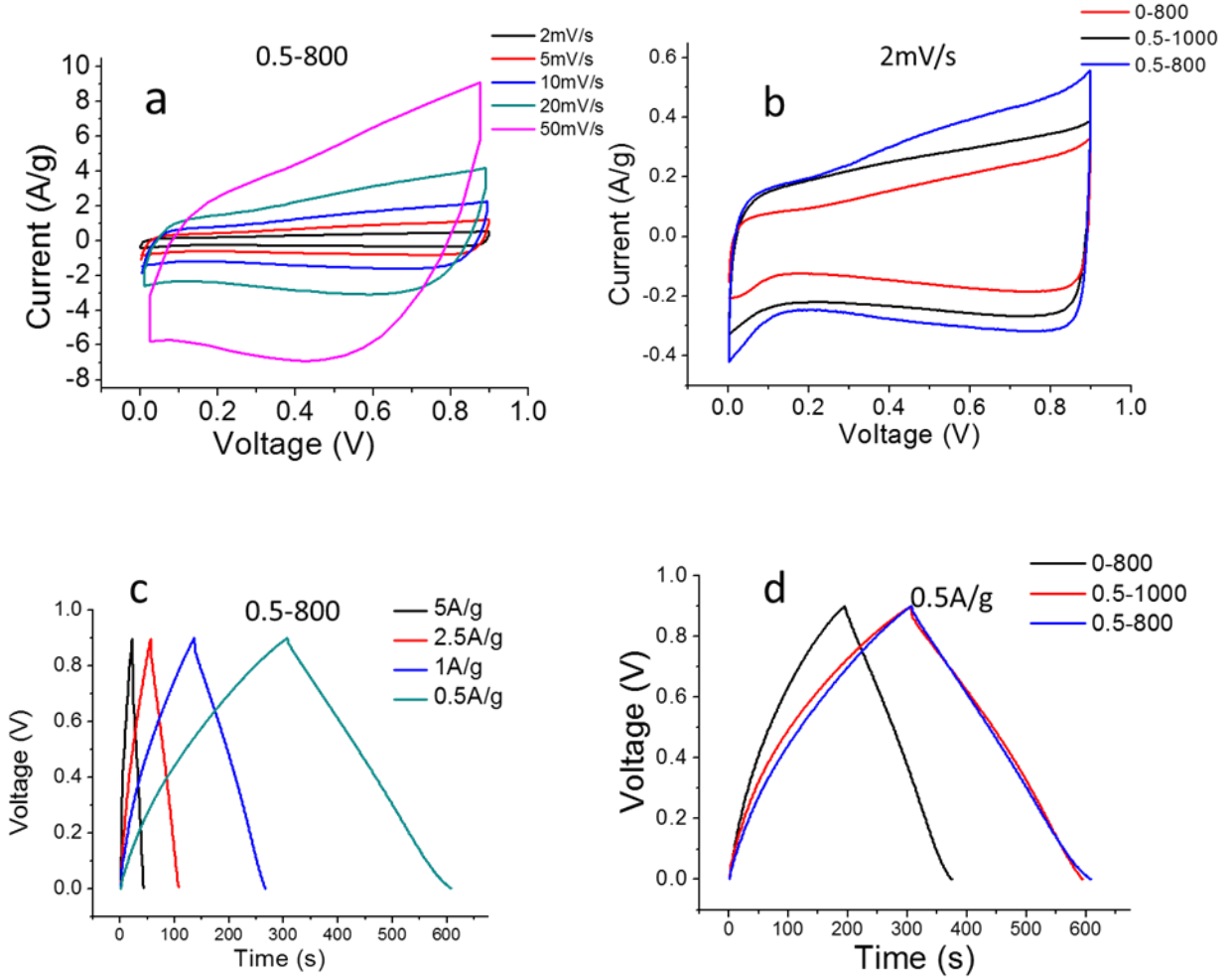


Figure 2.8: Supercapacitance behavior of nitrogen doped carbon measured in a three-electrode system using 6 mol L^{-1} KOH solution as electrolyte within the potential range: 0-0.9 V (vs. Ag/AgCl): (a) cyclic voltammetry curves at different scan rates for sample C0.5-800; (b) cyclic voltammetry curves at 2 mV/s for samples C0.5-800, C0.5-1000 and C0-800; (c) galvanostatic charge-discharge curves at various current densities for C0.5-800; (d) galvanostatic charge-discharge curves at 0.5 A/g for C0.5-800, C0.5-1000 and C0-800

C0-800.

To evaluate the advantages of the nitrogen doped carbon, the supercapacitor performance of all samples was measured in a three-electrode system. The tests were performed using 6M KOH solution as the electrolyte and measured against Ag/AgCl reference electrode. Fig. 2.7.a shows the cyclic voltammetry (CV) curves of sample C0.5-800 at scan rates from 2 to 50 mV/s. Figure 2.7.b shows the CV curves at low scan rate of C0.5-800, C0.5-1000 and compared to the carbon without nitrogen dopant C0-800. The curves in figure 2.7.a and b with scan rate lower than 20mV/s display a typical quasi-rectangular type loops and the curves of nitrogen doped carbon show clearly visible higher redox current at around 0.6V compared to C0-800, indicating the presence of both electrochemical double layer capacitance (EDLC) and pseudocapacitive effect due to a variety of redox reactions of the N and/or O functional groups in the carbon lattice with the electrolyte ions.[16,17] These groups can improve the surface affinity and therefore maximize the electroactive surface area of the obtained carbon.[18] As the scan rate reaches 50 mV/s, the shape of CV curve becomes a distorted triangle due to pseudocharge-transfer resistance and ion retardation within ultrafine micropores. The CV curves also display sharp current loops close to the upper potential limit, which could be ascribed to the charge-transfer from water decomposition with oxygen evolution. Additional charges from the oxygen evolution reactions accumulating on the carbon electrode surface resulted in higher current. [19] In addition to the cyclic voltage test, we also did galvanostatic charge–discharge (CP) test on all of the carbon samples. Figure. 2.7.c shows the galvanostatic charge–discharge curves of nitrogen doped carbon C0.5-800 at different current densities. Figure 2.7.d displays the CP curves at low current density of

C0.5-800, C0.5-1000 and C0-800. All the CP curves display a typical triangular shape with very small internal resistance drops (IR drops, less than 10mV at low current density). The CP curves are not exactly symmetrical but slightly distorted due to the pseudocapacitive effect of the N and O functional groups, which is consistent with the shape of CV curves. Since the galvanostatic charge/discharge method is widely recognized as the most accurate technique for supercapacitor testing, specific capacitance (C_s) of all carbon samples was calculated from the discharge curves according to equation (2.1):

$$C_s = \frac{I\Delta t}{m\Delta V} = \frac{I}{mK}$$

where I , Δt , m , ΔV and K are the applied current, discharge time, mass of the active electrode material, the voltage change excluding the IR drop during the discharge process and the slope of the discharge curve, respectively. [20] The results of specific capacitance calculated from the curves at 0.5A/g current density are listed in Table. 2.5.

Table. 2.5 Specific Capacitance of All Nitrogen-Doped Carbons at Low Current Density

Sample	Capacitance (F/g)	Sample	Capacitance(F/g)
0.1-800	183	0.1-1000	164
0.2-800	211	0.2-1000	174
0.3-800	199	0.3-1000	179
0.5-800	238	0.5-1000	191
1.0-800	179	1.0-1000	181

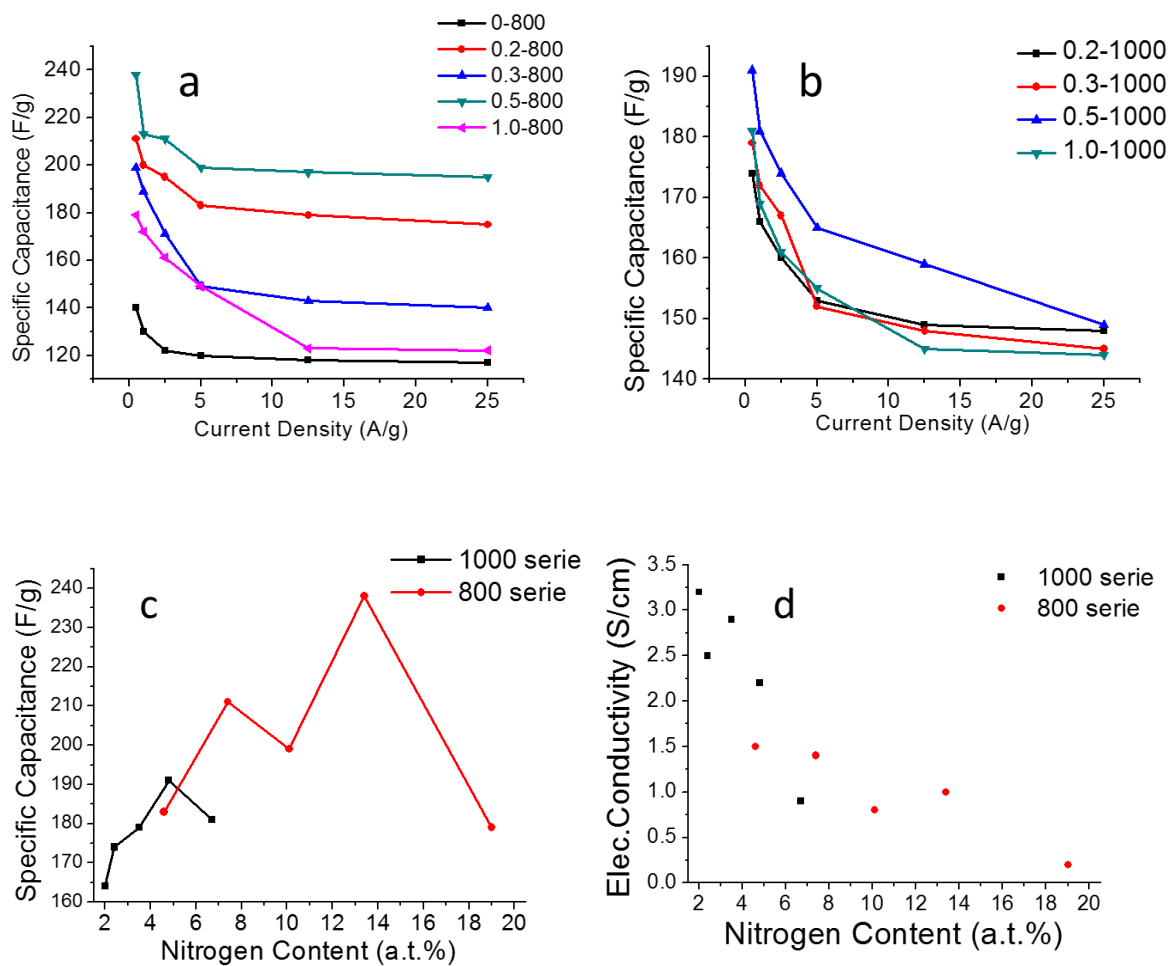


Figure 2.9: Specific capacitance at various current density of the 800 carbon series (a) and the 1000 carbon series (b); specific capacitance plotted against nitrogen content; (d)

electrical conductivities of nitrogen doped carbons as a function of nitrogen content. From Table 2.5 and Figure 2.9.a and 2.9.b, it is obvious that the nitrogen doped carbons have much higher capacitance than the C0-800 carbon which was synthesized similarly but without nitrogen doping, especially for the 0.5-800 which has specific capacitance of 238F/g at current density of 0.5A/g compared to 140F/g of the 0-800. The ideal supercapacitor is supposed to transport same energy at any current loading without losing its capacity. Therefore, specific capacitance at different current densities was calculated and plotted in Figure 2.9.a and b. In general, the obtained nitrogen doped carbons have high capacitance (over 180F/g) at low current density with high capacitance retention of around 80% at current density up to 25A/g. These results confirmed that the nitrogen incorporation in these carbon samples highly increased their capacitance while maintaining good capacity at different rates. Meanwhile, nitrogen doped carbons pyrolyzed at 800°C have higher specific capacitance than the 1000°C carbon series. This mainly attributes to the types of nitrogen and oxygen groups that exist in 800 carbons series, both of which are favorable towards good supercapacitor performance. Within each temperature series, as shown in Figure 2.9.c, an increase followed by decrease in capacitance was observed when plotted against nitrogen atomic contents, which makes the 0.5 sample the highest one in each series. We believe this is due to a steep fall in electrical conductivity as well as the shrinkage in surface area that counteracts the increased pseudocapacitance as the doping increases. Figure 2.9.d shows the relationship between nitrogen content and electrical conductivity measured using a 4-point probe electrical conductivity measurement set up.

2.3.5 Effects of Iodine Pretreatment

In order to study the effects of iodine pretreatment, carbons C0.3-800, C1.0-800, C0.3-1000 and C1.0-1000 were prepared with and without the pretreatment. To visualize the influence of the iodine pretreatment on the structure of the final carbon network, figure 2.10 shows the nitrogen adsorption-desorption isotherms (a, c) and BJH adsorption pore-size distributions (b, d) of nitrogen doped carbons synthesized with and without the iodine pretreatment. In general, from figure 2.10.a and c, it is obvious that iodine pretreatment decreases the surface area of the obtained carbon due to the increase in nitrogen incorporation and results in a less developed mesoporosity. However, pore size distribution plots (Figure 2.10.b and d) still display a sharper distribution of pore size centered at ~5-6 nm in agreement with the original silica nanoparticle size, especially after iodine treatment. This means that iodine and air pretreatments do not affect the pore structure to a significant extent.

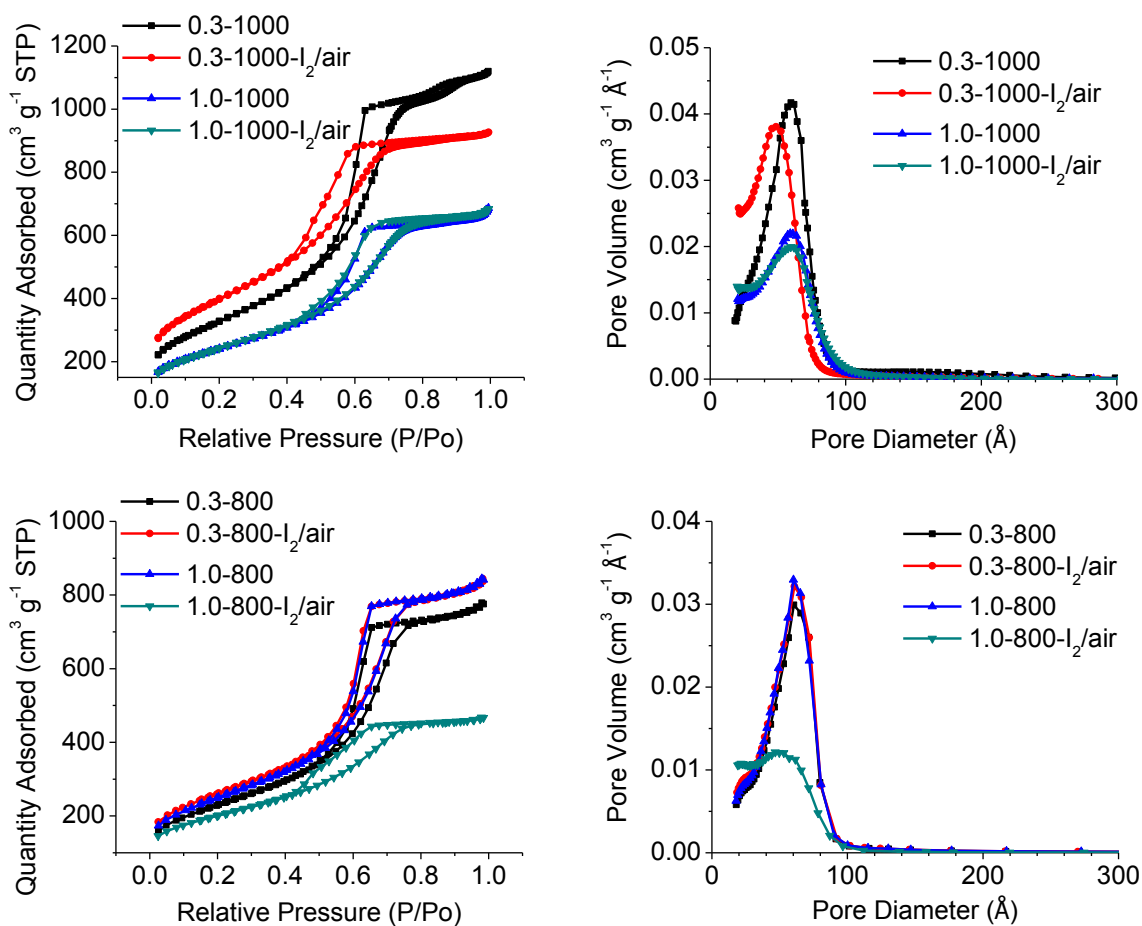


Figure 2.10: Nitrogen adsorption-desorption isotherms (a, c) and BJH adsorption pore-size distributions (b, d) of nitrogen-doped carbons synthesized with and without the iodine pretreatment, respectively.

The major difference between samples with and without the iodine pretreatment is the nitrogen content, which was revealed by XPS and listed in Table 2.6. At each ratio, a further increase was obtained after applying the iodine and air stabilization treatments. It increased from 5 at. % to 7.5 at. % for C0.3-1000 sample and from 8.9 at. % to 11.7 at. % for C1.0-1000 sample. For the 800 °C series, the nitrogen content increased from 11.3 at. % to 14.4 at. % and from 17.2 at. % to 22.5 at. %, for the C0.3-800 and C1.0-800 samples, respectively. Iodine pretreatment improves the thermal stability of the

precursors by forming a more cross-linked and cyclized structure due to dehydrogenation or dehydration reactions, preventing their volatilization during carbonization at elevated temperatures [21, 22]. In our case, since cyanamide and its polymerization product carbon nitride both decompose above 600 °C, iodine pretreatment could get the precursor mixture thermally stabilized by probably polymerizing cyanamide along with sucrose, which explain the higher retention of nitrogen after carbonization in all samples. However, for these samples with pretreatment, the increase in nitrogen content doesn't result in absolute increase in capacitance even though the type of nitrogen and oxygen functional groups are basically the same as the ones without pretreatment. We consider it is the same reason discussed in 2.3.4 that the dramatic decrease in electrical conductivity as well as the shrinkage in surface area counteracts the increased pseudocapacitance as the nitrogen doping increases. Even though the iodine pretreatment doesn't result in large increase of supercapacitor performance, it provides a strategy to synthesize nitrogen doped carbon with nitrogen content up to 22.5%, which is higher than most nitrogen doped carbon reported till now, and should be promising in other application fields such as CO₂ adsorption or electrocatalysis.

Table 2.6 Chemical Composition and Capacitance of Samples With/Without Iodine Pretreatment

Sample	N	C	O	Capacitance
	at. %	at. %	at. %	(F g ⁻¹)
0.3-1000	5.0	83.0	9.2	180
0.3-1000-I₂/air	7.5	78.8	11.1	209
1.0-1000	8.9	74.8	11.2	179
1.0-1000-I₂/air	11.7	77.3	7.6	158
0.3-800	11.3	73.1	13.0	200
0.3-800-I₂/air	14.4	67.9	14.2	203
1.0-800	17.2	67.1	12.3	177
1.0-800-I₂/air	22.5	58.8	12.6	157

2.4 Conclusions

A novel strategy to synthesize nitrogen doped mesoporous carbons via ice- templating using cyanamide as the nitrogen precursor, sucrose as the carbon source and colloidal silica as the hard template was developed. The obtained carbon possessed high surface (765 ~ 1028m²·g⁻¹) and high pore volume (1.00~2.27cm³·g⁻¹), uniform porosity (5-6nm) and high nitrogen content (up to 22.5 a.t. %). More importantly, the nitrogen incorporation can be easily tailored by controlling the cyanamide to sucrose weight ratio, changing the carbonization temperature from 800 °C to 1000°C or employing the iodine pretreatment step, which remarkably increases the nitrogen content after carbonization.

XPS analysis confirmed the presence of nitrogen mainly in the form of pyridinic and pyrrole/pyridone-N nitrogen regardless of the carbonization temperature and the cyanamide fraction, which would generate additional pseudocapacitance for supercapacitor applications. Different types of oxygen dopants were observed at carbonization temperatures of 800 °C and 1000 °C. Due to their high surface area, appropriate mesopore size together with large number of electrochemically active nitrogen and oxygen groups in the carbon framework, when tested as electrodes in a three-electrode supercapacitor system, these doped carbons exhibited high specific capacitance of up to 238 F g⁻¹ with good capacity retention at high rates (up to 80% at 25A/g), suggesting that these nitrogen doped mesoporous carbons are promising electrode materials for supercapacitor applications especially in occasions demanding high power.

REFERENCES

- [1] L. Estevez, R. Dua, N. Bhandari, A. Ramanujapuram, P. Wang and E. P. Giannelis. *Energy Environ. Sci.*, **6**: 1785 (2013).
- [2] S. Hwang, S. Lee and J-S. Yu, *Applied Surface Science*, **253(13)**:5656-9 (2007).
- [3] A. Thomas, A. Fischer, F. Goettmann, M. Antonietti, J-O. Muller and R. Schlogl, *J. Mater. Chem.*, **18(41)**:4893–908 (2008).

- [4] B. Jurgens, E. Irran, J. Senker, P. Kroll, H. Muller and W. Schnick, *J. Am. Chem. Soc.*, **125(34)**:10288–300 (2003).
- [5] N. Miyajima, S. Dohi, T. Akatsu, T. Yamamoto, E. Yasuda and Y. Tanabe, *Carbon*, **40(9)**:1533-9 (2002).
- [6] Z. Bashir, *Carbon*, **29(8)**:1081-90 (1991).
- [7] K. Parvez, S. Yang, Y. Hernandez, A. Winter, A. Turchanin and X. Feng, *ACS nano.*, **6(11)**:9541-50 (2012).
- [8] UK. Fatema, AJ. Uddin, K. Uemura and Y. Gotoh, *Textile Research Journal* (2010).
- [9] Luis Estevez, SYNTHESIS AND CHARACTERIZATION OF NANO-HYBRID SYSTEMS WITH INDUCED POROSITIES VIA ICE TEMPLATION [PhD thesis] (2013).
- [10] H-L. Guo, P. Su, XF. Kang and S-K Ning, *J. Mater. Chem. A*, **1**: 2248 (2013)
- [11] F. Tuinstra and J.L. Koenig, *J. Chem. Phys.*, **53**:1126 (1970).
- [12] T. Jawhari, A. Roid and J. Casado, *Carbon*, **33**: 1561 (1995).
- [13] D-W .Wang, F .Li, L-C .Yin, X .Lu, Z-G .Chen and IR .Gentle, *Chem Eur J.*, **18(17)**:5345–51 (2012).
- [14] R. Arrigo, M. Hävecker, S. Wrabetz, R. Blume, M. Lerch and J. McGregor, *J. Am. Chem. Soc.*, **132(28)**:9616-30 (2010).
- [15] L. Wan, J. Wang, Y. Sun, C. Feng and K. Li, *RSC Adv.*, **5(7)**:5331-42 (2015).

- [16] D. Hulicova-Jurcakova, M. Kodama, S. Shiraishi, H. Hatori, Z. H. Zhu and G. Q. Lu, *Adv. Funct. Mater.*, **19**: 1800–1809 (2009).
- [17] W. Li, F. Zhang, Y. Dou, Z. Wu, H. Liu, X. Qian, D. Gu, Y. Xia, B. Tu and D. Zhao, *Adv. Energy Mater.*, **1**: 382–386. 44 (2011).
- [18] P. J. Hall, M. Mirzaeian, S. I. Fletcher, F. B. Sillars, A. J. R. Rennie, G. O. Shitta-Bey, G. Wilson, A. Cruden and R. Carter, *Energy Environ. Sci.*, **3**: 1238–1251 (2010).
- [19] Y. Wang, R. Yang, Y. Wei, ZJ. Zhao and M. Li, *RSC Adv.*, **4**: 45318 (2014)
- [20] L. Qie, WM. Chen, HH. Xu, XQ. Xiong, Y. Jiang, F. Zou, XL. Hu, Y. Xin, ZL. Zhang and YH. Huang, *Energy Environ. Sci.*, **6**:2497 (2013).
- [21] M. Sashio and M. Tanaka., *Journal of Polymer Science: Polymer Chemistry Edition*, **23(3)**:905-9 (1985).
- [22] J. Yamashita, Y. Soneda, M. Kodama, H. Hatori, M. Shioya, *J. Mater. Sci.*, **39(4)**:1463-6 (2004).

CHAPTER 3

ACTIVATION OF NITROGEN DOPED CARBONS FOR SUPERCAPACITOR ELECTRODE MATERIAL

3.1 Introduction

Supercapacitor stores energy physically at the electrode–electrolyte interface based on electrochemical double-layer mechanism, therefore a higher specific surface area would lead to better supercapacitor performance for the carbon-based electrode materials. In order to enhance the surface area and microporosity of the nitrogen doped carbon demonstrated in Chapter 2, an activation step was involved and the results are presented in this Chapter. The activation process introduced microporosity to the nitrogen doped carbon, along with macropores from the ice templating and mesopores from the silica template. The strategies to form these three different pore scales is displayed in Figure 3.1. The activation of carbon materials have long been studied and used commercially. In the last few decades, many papers have reported on the activation of carbon-based material for various applications. Among a variety of activation techniques available, we focused on CO₂ activation, which is typical of physical activation.

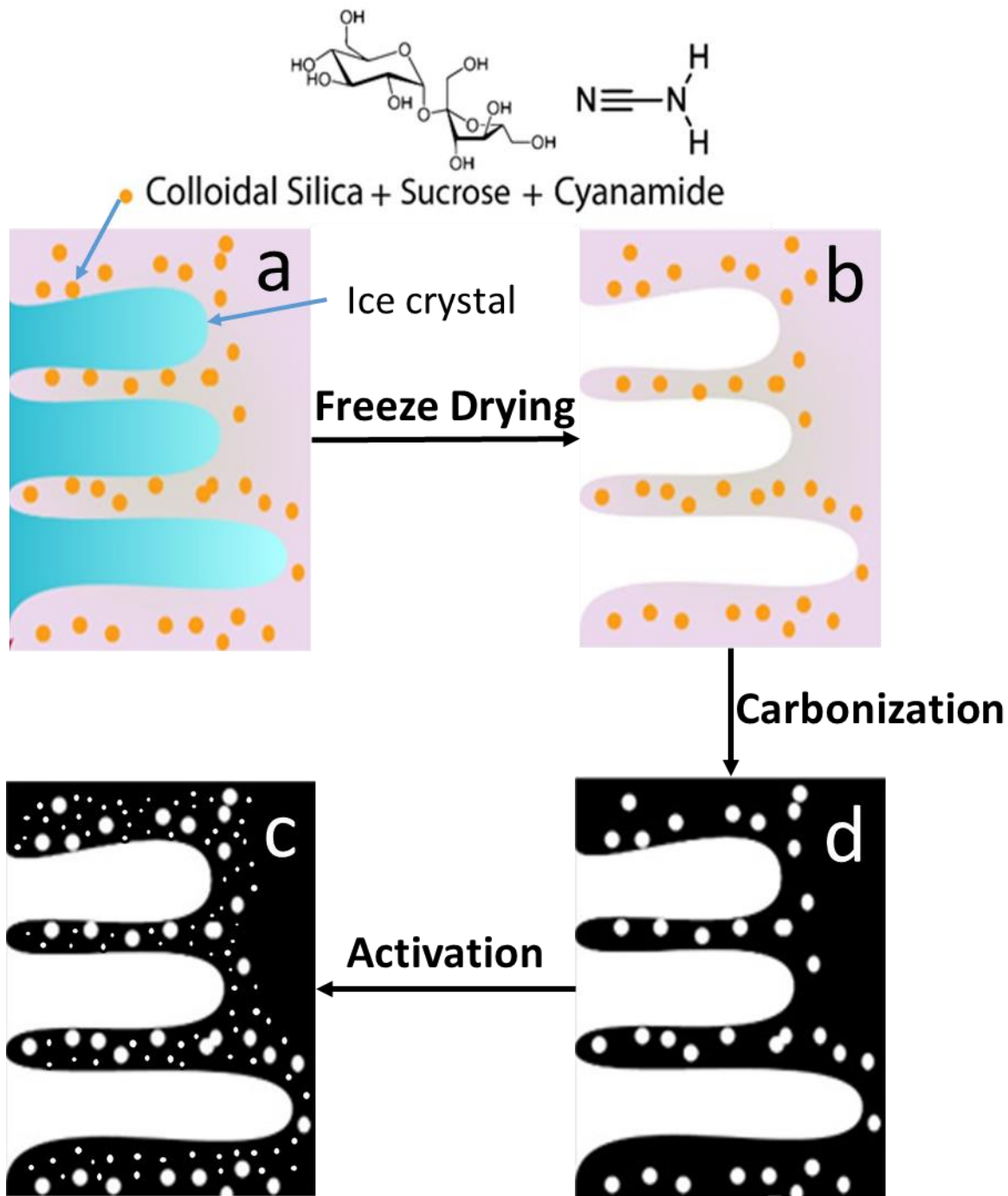


Figure 3.1: Schematic showing the four basic steps and material prepared after each step. The four steps shown clockwise from top left are: a (top view) ice templating - ice front movement through the sucrose, cyanamide and colloidal silica aqueous suspension forming ice crystals; b (top view) freeze drying - the sucrose-cyanamide-silica composite

material with macropores after removal of ice;c (top view) carbonization and silica etching results in macro-mesopore dominated carbon; d Physical activation, to introduce micropores.[1]

During the CO₂ activation process, the carbon material is maintained at high temperature (typically 800-1000°C) under a flow of CO₂ gas for a period of time (usually for hours).

[2] The reaction that happens is shown as Equation 3.1 where carbon atoms are released from the surface of carbon materials:



As demonstrated in Equation 3.1, this reaction is endothermic while generally the oxidation process of carbon is highly exothermic and hard to control. Therefore the activation process can be considered as a controlled oxidation of the carbon. It is worth mentioning that the exact mechanism of the activation process is not as simple as what equation 3.1 indicates and it is beyond the scope of our work. In fact, as reported in literature, there is some sort of selection process as CO₂ won't gasify the first carbon atom it encounters; rather, there may possibly be as many as 10¹⁷ carbon atoms encountered before one is gasified [2]. In this work, we employed the activation process for the purpose of increasing the surface area and porosity of nitrogen doped carbons and therefore improving their supercapacitor performance. To that end, we followed a standard activation technique, which has long been used in our group and previously described in the literature [3].

3.2 Experimental Section

3.2.1 Activation Procedure of Nitrogen Doped Carbons

The nitrogen doped samples obtained as described in Chapter 2 (after drying in vacuum oven) are heated first under an inert atmosphere (argon in this work) up to a temperature of 950 °C, whereupon the inert gas is replaced by CO₂ at a flow rate of 50 cc/min. The time for activation is 1 h.

3.2.3 Characterization

Raman spectra were recorded with a Renishaw InVia Confocal Raman microscope. Nitrogen sorption isotherms were obtained at 77K using Micromeritics ASAP 2460 analyzer. The Brunauer-Emmett-Teller (BET) model was applied to calculate the specific surface area and Barrett-Joyner-Halenda (BJH) model was used to obtain pore size distributions and total pore volume from the adsorption branch of isotherms. The chemical composition and bonding information of C, N and O was analyzed by X-ray photoelectron spectroscopy (XPS) using a Surface Science Instruments SSX-100 operating pressure of $\sim 1 \times 10^{-8}$ Torr.

3.2.4 Electrochemical Measurements

All nitrogen doped carbons were tested as electrochemical supercapacitors and all electrochemical experiments were carried out on a Solatron electrochemical workstation in a three-electrode system at room temperature. To prepare the electrodes, a thick slurry consisting of 80 wt % obtained carbon material, 10 wt % carbon black (SuperP), and 10 wt % polyvinylidene fluoride (PVDF) as binder, respectively, using N-methylpyrrolidone (NMP) as the solvent was mixed uniformly, pressed onto a nickel foam (current collector) and dried at 80°C in oven. The mass of nitrogen doped carbon on each nickel foam was around 3.0~6.0 mg in an area around 1.0 cm². In a three-electrode set up, platinum wire was used as the counter electrode, Ag/AgCl as the reference electrode, and sample carbon coated nickel foam as the working electrode with 6 M KOH aqueous solution as the electrolyte. Cyclic voltammetry (CV) curves were carried out within the potential range of 0-0.9 V vs Ag/AgCl by varying the scan rate from 2 to 50 mVs⁻¹. Charge-discharge measurements were tested galvanostatically at 0.5-25A g⁻¹ within a voltage range of 0-0.9 V vs Ag/AgCl.

3.3 Results and Discussion

3.3.1 Activation Conditions of Nitrogen Doped Carbons

To figure out the proper activation temperature and time, we activated sample C0.5-800 under four different conditions: 800 °C for 2h, 850 °C for 2h, 900 °C for 2h and 950 °C for 1h. The results of specific surface area for the final activated carbon obtained after these four treatments are listed in Table 3.1.

Table 3.1 Specific surface area and yield of final carbons for different activation conditions

Activation Condition	Yield (%)	BET surface area (m ² /g)
800 °C for 2h	78	1096
850 °C for 2h	50	1367
900 °C for 2h	28	1475
950 °C for 1h	20	1760

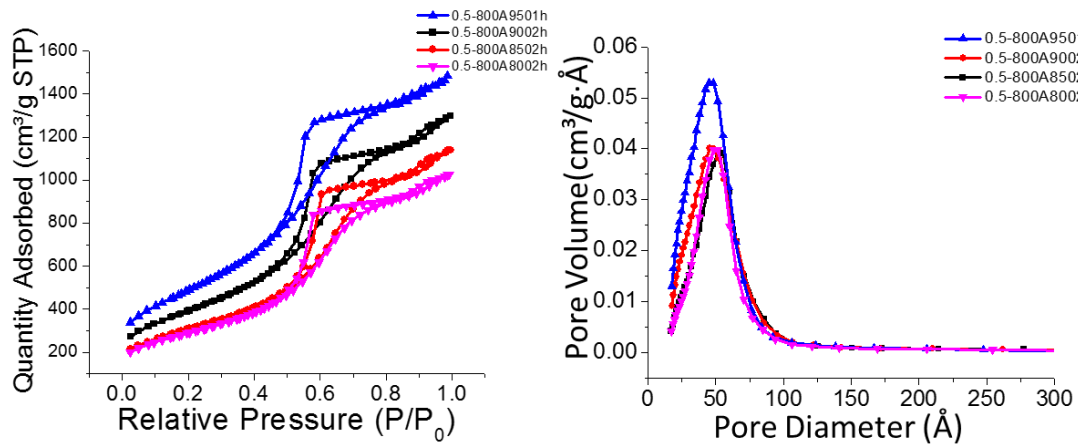


Figure 3.2: Nitrogen adsorption-desorption isotherms and BJH adsorption pore-size distributions of C0.5-800 activated under different conditions.

From Figure 3.2 and Table 3.1, it is obvious that the carbon sample activated at 950 °C for 1h has the highest specific surface area and the sharpest distribution of pore size centered at ~5-6 nm. Compared to specific surface area of 923 m²/g for the pristine sample C0.5-800, the 1h activation at 950 °C almost doubled the value, which confirmed that this condition is sufficient for the activation process. However, if the nitrogen doped carbon was activated for longer time under 950 °C, the yield of the final material was very low (less than 10%). The relationship between the yield and the nitrogen content in the pristine none-activated carbon is shown in Figure 3.3. The carbon framework of these nitrogen doped carbons is expected to be less stable than that without nitrogen and thus these nitrogen doped carbons cannot be activated as long as reported previously by our group (up to 4h).[4]

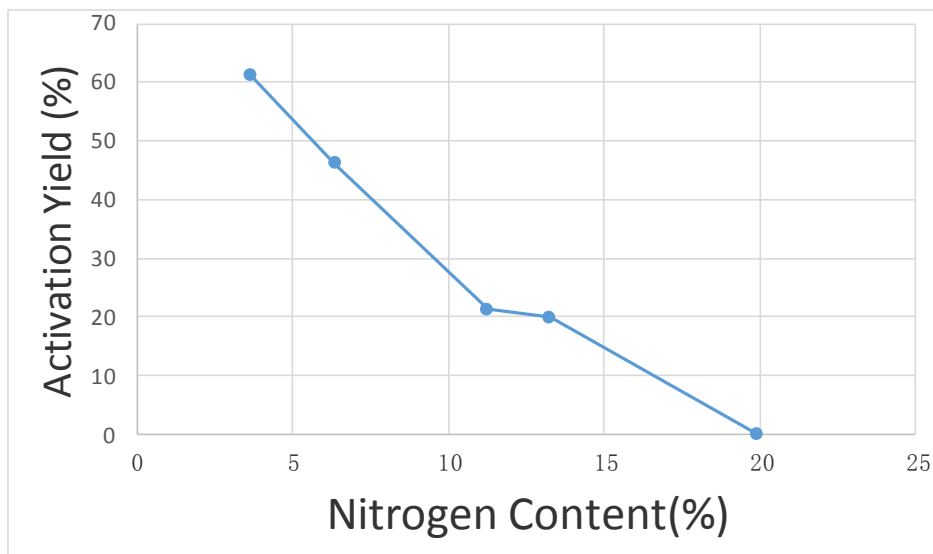


Figure 3.3: Relationship between the yield and the nitrogen content in the pristine non-activated carbon

3.3.2 Structural Analysis of Activated Nitrogen Doped Carbon

Most of the nitrogen doped carbons synthesized using the strategy discussed in Chapter 2 were activated for 1h at 950 °C under a CO₂ gas flow except the 1.0-800 and 1.0-1000, which have much higher nitrogen content than other samples but that under this activation condition the yield is too low (less than 5%). We believe that for nitrogen doped carbon with nitrogen higher than 15 a.t. %, lower activation temperature or less activation time should be applied to obtain enough amount of final materials. For the purpose of this study, we only did activation on the samples synthesized with 0.1, 0.2, 0.3 and 0.5 cyanamide fraction in the precursor mixture. The specific surface area and pore volume of these samples before and after activation are listed in Table 3.2. Figure 3.4 shows the nitrogen adsorption-desorption isotherms curves and BJH adsorption pore-size distributions curves for these samples.

Table 3.2 Surface area and pore volume of nitrogen doped carbons before and after activation

Sample	BET surface area (m ² /g)	V _{meso} (cm ³ /g)	V _{micro} (cm ³ /g)	Sample	BET surface area (m ² /g)	V _{meso} (cm ³ g ⁻¹)	V _{micro} (cm ³ g ⁻¹)
0.1-800NA	1028	2.06	0.023	0.1-800A	1773	2.43	0.017
0.2-800NA	1008	1.67	0.009	0.2-800A	1998	2.98	0.043
0.3-800NA	979	1.39	0.004	0.3-800A	1705	2.01	0.009
0.5-800NA	923	1.27	0.009	0.5-800A	1760	2.34	0.003
0.1-1000NA	1009	2.27	0.030	0.1-1000A	1546	2.67	0.110
0.2-1000NA	996	1.96	0.012	0.2-1000A	1938	2.88	0.039
0.3-1000NA	974	1.85	0.021	0.3-1000A	1850	2.71	0.046
0.5-1000NA	975	1.58	0.012	0.5-1000A	1814	2.59	0.012

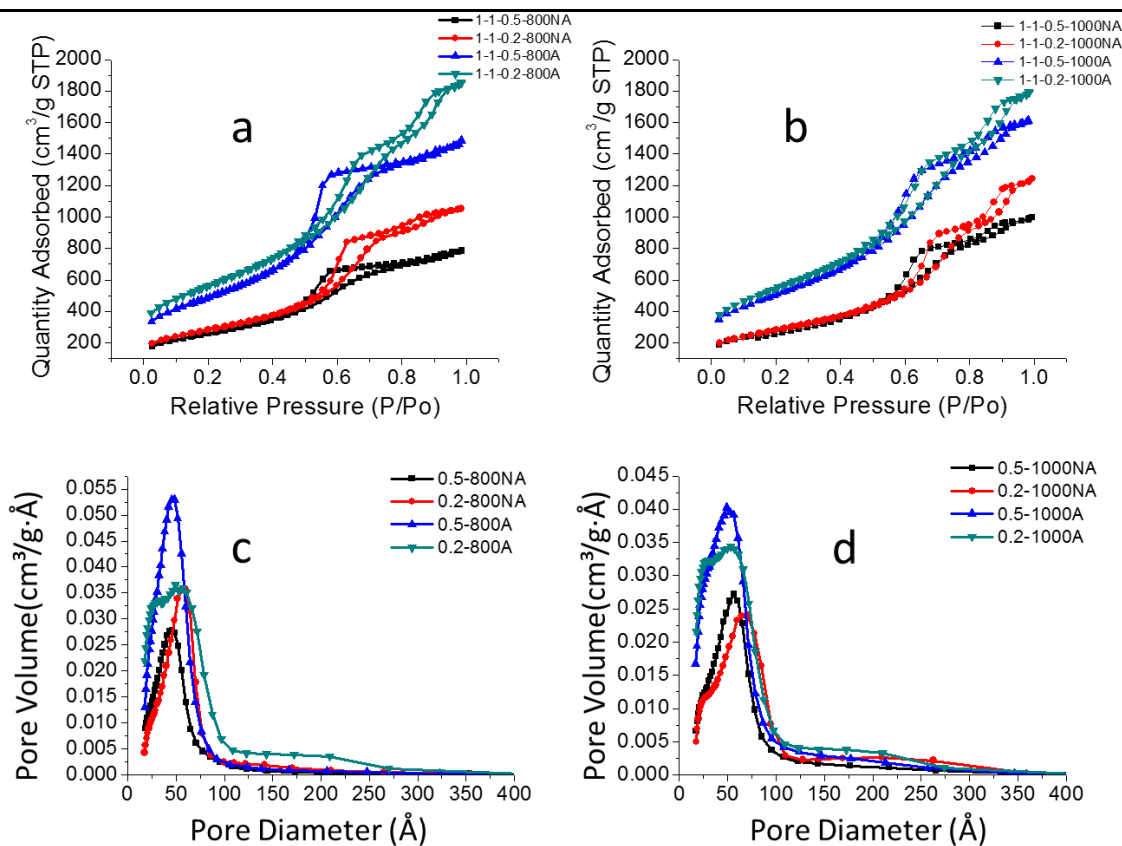


Figure 3.4: Nitrogen adsorption-desorption isotherms (a, b) and BJH adsorption pore-size distributions (c, d) of nitrogen doped carbons carbonized at 800 and 1000 °C before and

after activation process, respectively.

In general, as discussed previously, CO₂ is slowly gasifying the carbon atoms, which leads to not only the increase of specific surface area but also mesopore volume. The specific surface area of nitrogen doped carbons increased by 750-950 m²/g and the pore volume of mesopores increased by 0.4-1.30cm³/g after the 1h activation. These activated nitrogen doped carbons have higher surface area and pore volume than most nitrogen-doped carbons reported in the literature (usually lower than 1500 m²/g). [5,6,7]

In figure 3.4.a and b, the activated samples and the non-activated ones display similar type IV isotherms with a clear capillary condensation step at around P/Po =0.5-0.7, which indicates the presence of mesoporous network in all obtained carbon materials. However, the activated nitrogen doped carbons seem not to follow the same trend as the non-activated ones. The value of specific surface area and pore volumes is independent from the nitrogen content instead of decreasing as the nitrogen content increased. Pore size distribution curves as plotted in Figure 3.4c and d demonstrate the difference in porosity between the activated materials and the non-activated ones. The activated ones not only show higher volume of pore size centered at ~5-6 nm than the pristine non-activated samples but also obviously have higher distribution of pore size less than 5nm, as can be seen from the edge of the limits of the BJH distribution curves where a shoulder from 2-4 nm appears after activation, which indicates the increase in microporosity in the activated nitrogen doped carbons.

For further analyses of the influence of activation process on the nitrogen doped carbon structure, Raman spectroscopy was employed. The Raman spectra of samples before and after activation show very similar patterns with three peaks, among which two strong

peaks at $\sim 1350\text{ cm}^{-1}$ (D-Band) and $\sim 1580\text{ cm}^{-1}$ (G-Band) can be seen clearly in Figure 3.5. The D-band is associated with vibrations of carbon atoms with dangling bonds in plane terminations of the disordered graphite and thus is related to the disorder and defects in the structure. The G-Band is ascribed to the vibration of sp^2 bonded carbon atoms in a 2D hexagonal lattice, which is the stretching modes of C=C bonds of typical graphite. [8] Therefore, the relative intensities of these two peaks (I_D/I_G ratio) reflect the degree of graphitization of the carbon-based material. The exact number of I_D/I_G ratio for nitrogen doped carbon before and after activation are listed in Table 3.3. In general, the I_D/I_G ratio of nitrogen doped carbon changes only slightly after activation, which indicates that the activation step does not change the overall order/defects in the carbons.

Table 3.3 I_D/I_G Ratio for nitrogen doped carbon before and after activation

Sample	I_D/I_G Ratio	
	None Activated	Activated
0-800	1.0	1.1
0.2-800	1.4	1.5
0.5-800	1.6	1.5
0.5-1000	1.2	1.7

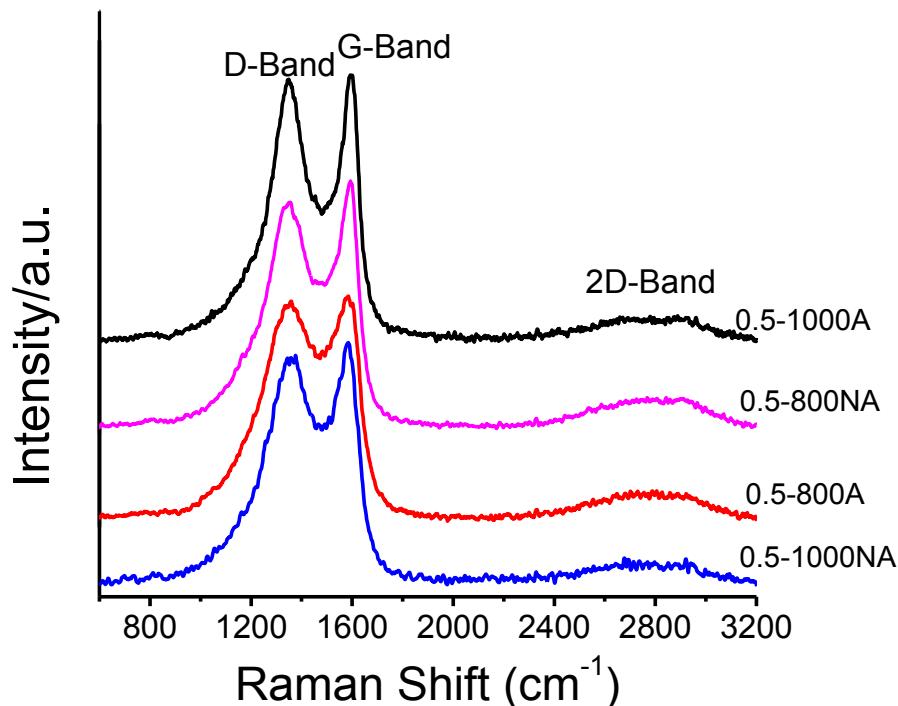


Figure 3.5: The Raman Spectra of the nitrogen doped carbon before and after activation

3.3.3 Chemical Composition of Nitrogen Doped Carbons

X-ray photoelectron spectroscopy (XPS) was used to investigate the chemical compositions of all samples before and after activation. The atomic content of C, N and O calculated from the XPS scans in all samples is listed in Table 3.4. The nitrogen content decreases significantly for the 800 carbon series after activation while only a slight reduction occurred for the 1000 carbon series. The change in nitrogen content for the 800 and 1000 carbon series is plotted in figure 3.6. It seems that no matter how high the nitrogen content in the pristine sample, it will reduce to around 2-5% after activation. This can be ascribed to the lack in stability of nitrogen functional groups at higher temperatures.

Further study is needed to figure out the exact mechanism of the activation process and its effect on composition.

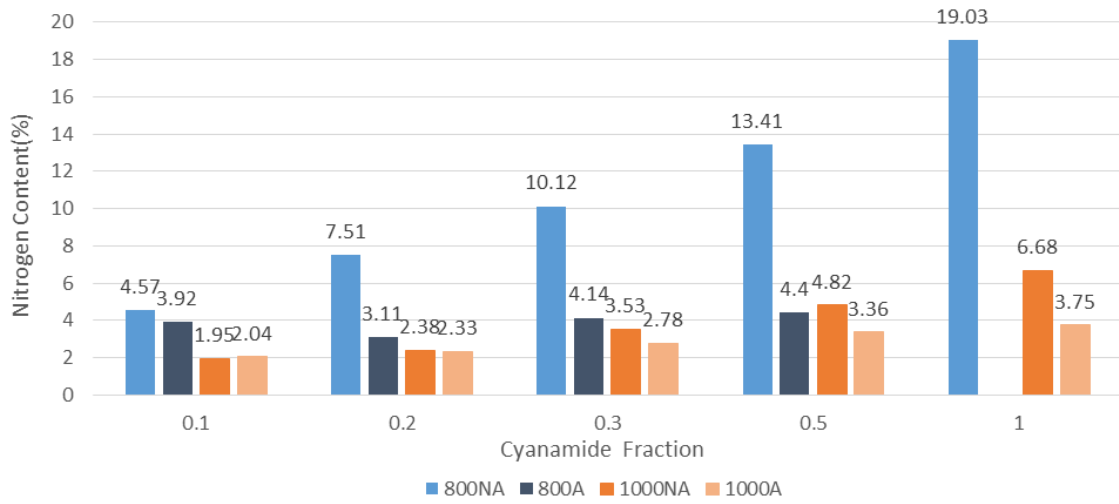


Figure 3.6: Nitrogen content in 800NA, 800A, 1000NA and 1000A carbon Series

Table 3.4 Atomic composition of samples before and after activation

Sample	N	C	O	Sample	N	C	O
	a.t.%	a.t.%	a.t.%		a.t.%	a.t.%	a.t.%
0.1-800NA	4.6	88.6	5.3	0.1-800A	3.9	87.7	6.7
0.2-800NA	7.4	80.0	8.2	0.2-800A	3.1	90.4	5.6
0.3-800NA	10.1	84.5	4.4	0.3-800A	4.2	88.6	6.2
0.5-800NA	13.4	80.4	4.5	0.5-800A	4.4	89.8	5.0
0.1-1000NA	2.0	92.9	4.2	0.1-1000A	2.0	93.5	4.3
0.2-1000NA	2.4	87.2	7.5	0.2-1000A	2.3	91.4	5.4
0.3-1000NA	3.5	89.6	5.2	0.3-1000A	2.8	93.8	2.9
0.5-1000NA	4.8	86.2	6.4	0.5-1000A	3.4	92.6	3.4

To reveal the influence of the activation process on the nature of nitrogen and oxygen dopants, we also investigated the high-resolution spectra of the individual nitrogen (Figure 3.7.a and b) and oxygen 1s (Figure 3.7c and d) peaks observed in XPS analysis. Unlike the pristine non-activated carbon, the nitrogen N 1s peak of the activated samples could only be resolved into two nitrogen peaks centered at 398.4 eV and 400.4 eV

representing pyridinic-N (N-6) and pyrrolic/pyridone-N (N-5), respectively. Also, the fraction of N-6 type increased significantly after activation, which accounted for over 80% of nitrogen in each activated samples. As discussed in section 2.3.3, only N-6 and N-5 are electrochemically active in alkaline electrolyte and thus the absence of N-X in the activated samples won't have influence on the pseudocapacitive effect. [9] For the types of oxygen dopant, the results of the activated samples are similar to the non-activated ones. As shown in table 3.5, for the 800 series, the dominant groups are still C=O (O-1), C-OH (O-4). The corresponding ones for the 1000 series are still quinone (O-1), C-O ether type (O-3). In summary, the activation process reduces the nitrogen content to a large extent for pristine samples with high nitrogen content and change the type of nitrogen dopant while it has limited influence on the oxygen content and the type of oxygen dopant.

Table 3.5 Characterization of the different types of nitrogen and oxygen dopants

Sample	N-6	N-5	N-6/N-5	O-1	O-2	O-3	O-4	O-5
	%	%		%	%	%	%	%
0.1-800A	18.4	81.6		-	35.5	-	49.8	14.7
0.2-800A	5.7	94.3		-	32.5	-	57.0	10.5
0.3-800A	14.0	86.0		-	21.7	-	57.6	20.7
0.5-800A	17.5	82.5		-	21.9	-	72.7	5.4
0.1-1000A	13.8	86.2		12.6	-	50.6	-	37.1
0.2-1000A	17.2	82.7		36.5	-	53.1	-	10.4
0.3-1000A	16.0	83.9		29.6	-	61.8	-	8.6
0.5-1000A	11.4	88.6		15.5	-	71.3	-	13.2

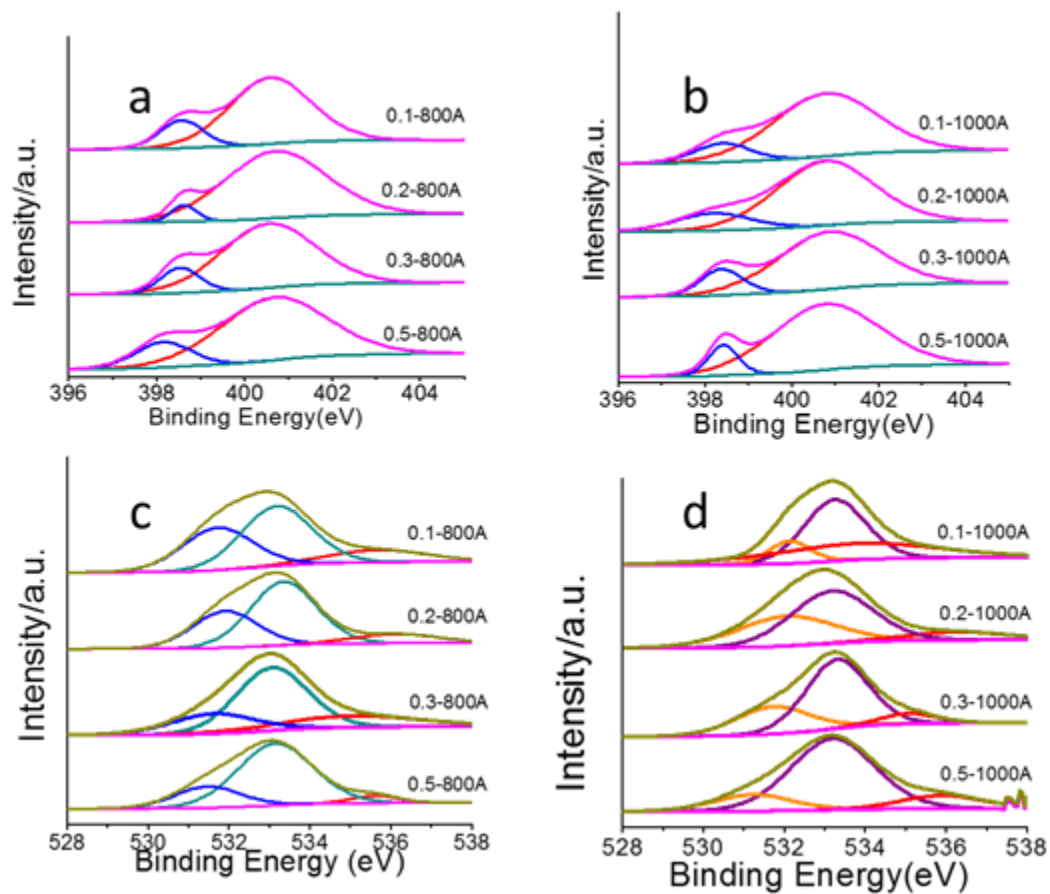


Figure 3.7: High-resolution N1s (a, b) and O1s (c, d) spectra, for the activated samples.

3.3.4 Supercapacitor Performance of Nitrogen Doped Carbons

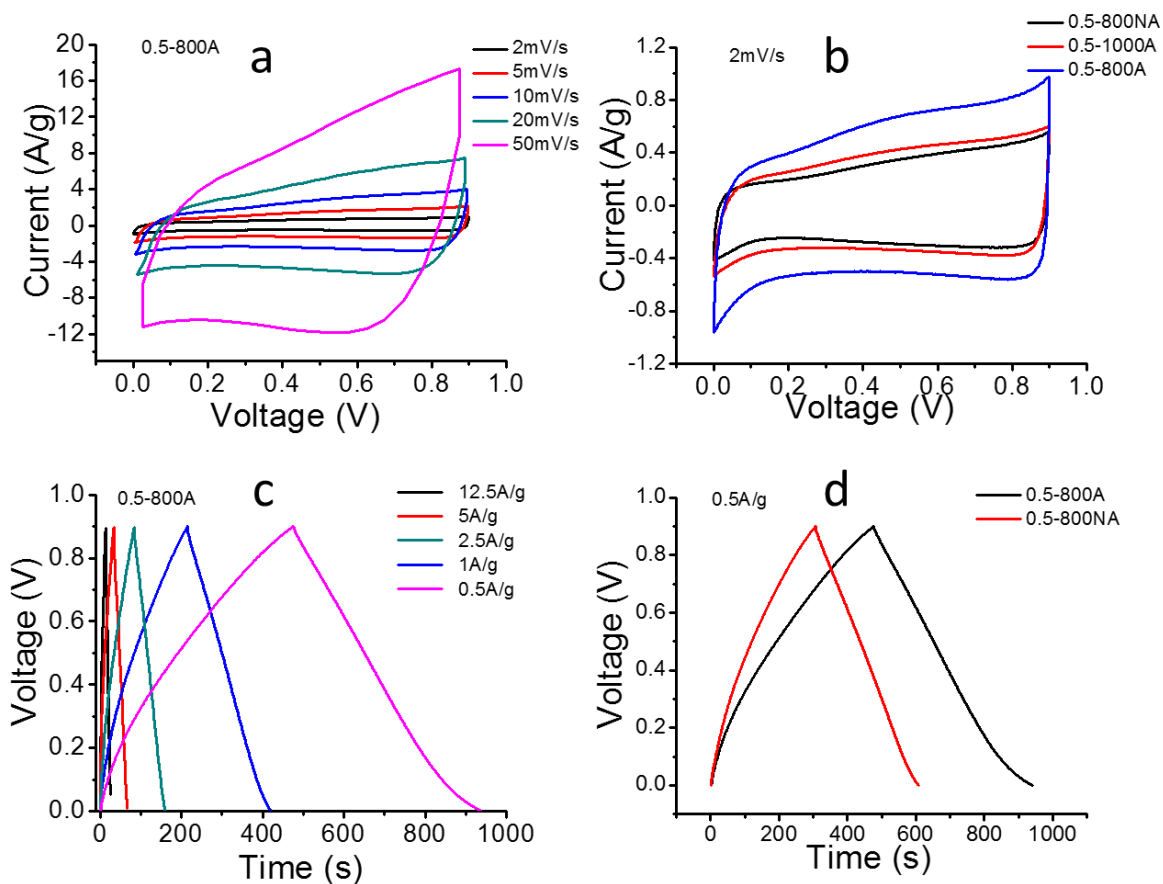


Figure 3.8: Supercapacitance behavior of activated nitrogen doped carbon measured (a) cyclic voltammetry curves at different scan rates for sample 0.5-800A; (b) cyclic voltammetry curves at 2mV/s for sample 0.5-800A, 0.5-1000A and 0.5-800NA; (c) galvanostatic charge–discharge curves at various current densities for sample 0.5-800A;

(d) galvanostatic charge–discharge curves at 0.5A/g for sample 0.5-800A and 0.5-800NA. To evaluate the advantages of activated nitrogen doped carbon, the supercapacitance performance of all activated samples was measured in a three-electrode system and tested under the same condition discussed in section 2.3.4. The curves in Figure 3.8.a and b of the activated samples 0.5-800A and 0.5-1000A display a similar quasi-rectangular shape as those non-activated nitrogen doped samples with clearly visible higher redox current at around 0.6V. The difference is that the CV loops of activated samples have much larger areas, indicating the increase of electrochemical double layer capacitance (EDLC) due to the increase in specific surface area and pore volume after activation. Figure. 3.8.c shows the galvanostatic charge–discharge curves of nitrogen doped carbon 0.5-800A at different current densities. Figure 3.8.d shows the CP curves at low current density of 0.5-800A and 0.5-800NA. Consistent with the CV results, the charge-discharge curves of activated samples display a similar triangular shape as the non activated ones with very small internal resistance drops (IR drops, less than 10mV at low current density). And again, under the same current density, the activated samples have longer discharge time than the none-activated ones, which means the activated samples have better performance. The results of specific capacitance calculated from the discharge curves at 0.5A/g current density are listed in Table. 3.6. Generally, activated samples have very high capacitance (over 200F/g), indicating the advantage of larger surface area and higher pore volume. The specific capacitance of nitrogen doped carbon increased by 20-80F/g after activation. Especially for sample 0.5-800A, the specific capacitance at 0.5A/g is 316F/g, which is higher than most nitrogen doped carbon sample reported. [10, 11, 12] Since the capacitance of sample 0-800A (i.e. carbon sample containing no nitrogen and activated

under the same conditions) is only 191F/g, the nitrogen doping plays a significant role in the capacitance of the sample.

Table. 3.6 Specific capacitance of nitrogen-doped carbons before and after activation at low current density

Sample	Capacitance (F/g)	Sample	Capacitance(F/g)
0-800NA	140	0-800A	191
0.1-800NA	183	0.1-800A	207
0.2-800NA	211	0.2-800A	248
0.3-800NA	199	0.3-800A	282
0.5-800NA	238	0.5-800A	316
0.1-1000NA	164	0.1-1000A	200
0.2-1000NA	174	0.2-1000A	239
0.3-1000NA	179	0.3-1000A	255
0.5-1000NA	191	0.5-1000A	262

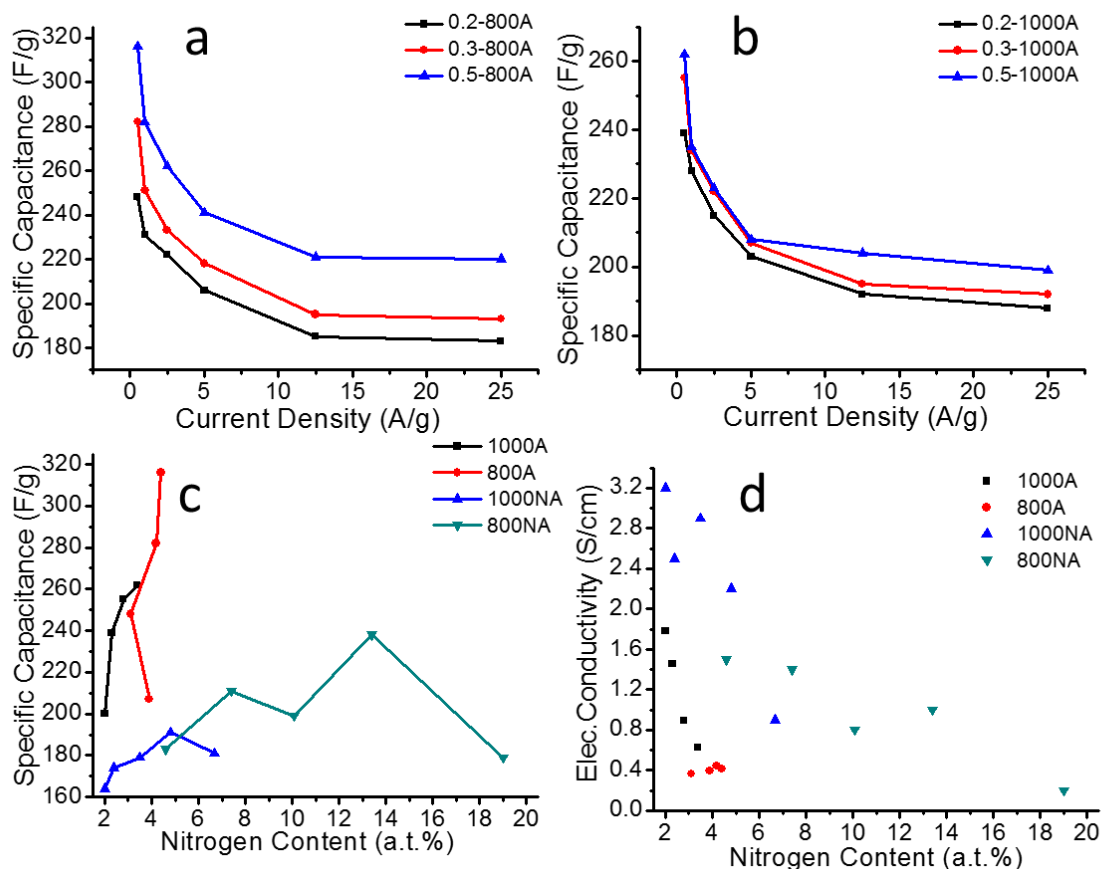


Figure 3.9: Specific capacitance at various current densities of the activated 800 carbon series (a) and the activated 1000 carbon series (b); specific capacitance plotted against nitrogen content; (d) electrical conductivities of nitrogen doped carbons as a function of nitrogen content.

Figure 3.9.a and 3.9.b show that after activation, these nitrogen-doped carbon still maintain high capacitance. At current density as high as 25A/g, all activated samples still show capacitance over 180F/g. These results confirmed that activation of nitrogen doped carbon not only increases their capacitance but also retain good capacity values

Meanwhile, from figure 3.9.c, it is obvious that the amount of nitrogen content still plays

a significant role on the final capacitance of activated carbon. Although activation treatment and nitrogen dopant would decrease the electric conductivity of the obtained material, these two modifications still lead to higher capacitance. Therefore, synthesis of higher nitrogen content (over 10 a.t. %) activated mesoporous carbon would be a future goal of this work. We also tested the long term stability of the synthesized carbons. The results are plotted in figure 3.10. After 600 cycles, the electrode still retain around 98% of its capacitance, indicating excellent long term stability of our nitrogen doped carbon as electrode material for supercapacitor.

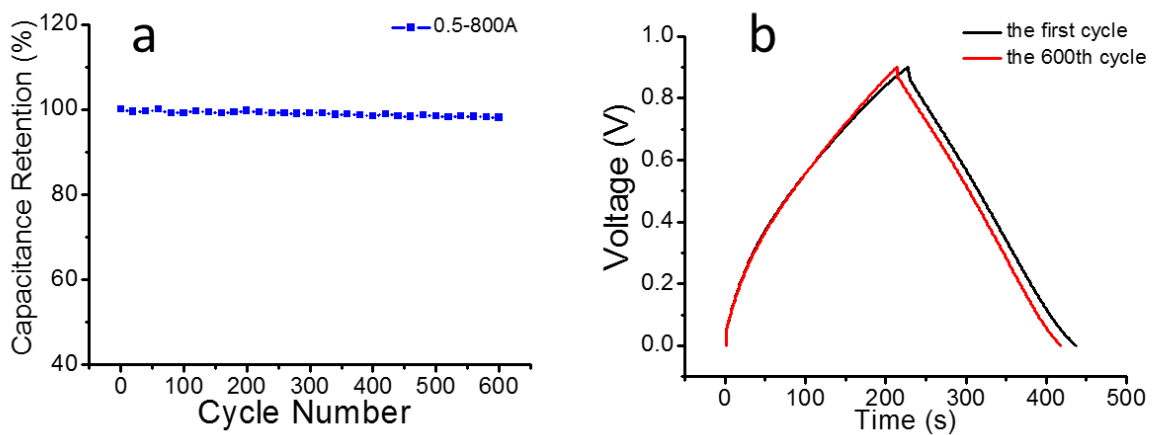


Figure 3.10: (a) cycling stability measured for 0.5-800A in three-electrode set up; (b) charge-discharge curve of the first and 600th cycle for 0.5-800A.

3.4 Conclusions

Activated nitrogen doped carbon with high specific surface area (up to 1998m²/g) and high pore volume (up to 2.98cm³/g) has been prepared via a physical activation process.

After CO₂ activation of the nitrogen doped carbon material synthesized using the strategy discussed in chapter 2, the obtained activated carbon possessed a large fraction of fine micropores with a fair nitrogen and oxygen content, leading to exceptional electrochemical properties. As the electrode material for supercapacitor, these activated nitrogen doped carbons exhibit superior capacity (up to 316F/g), good capacity at high rates (220F/g at 25A/g) and long-term cycle stability (98% retention after 600 cycle). As such the activated nitrogen doped carbon electrodes could find application in the energy storage field as supercapacitor electrodes.

REFERENCES

- [1] Luis Estevez, SYNTHESIS AND CHARACTERIZATION OF NANO-HYBRID SYSTEMS WITH INDUCED POROSITIES VIA ICE TEMPLATION [PhD thesis] (2013).
- [2] H. Marsh, FR. Reinoso, Activated Carbon, Elsevier Inc. (2006).
- [3] K. Xia, Q. Gao, J. Jiang and J. Hu, *Carbon*, **46**: 1718 (2008).
- [4] L. Estevez, R. Dua, N. Bhandari, A. Ramanujapuram, P. Wang and E. P. Giannelis. *Energy Environ. Sci.*, **6**: 1785 (2013).
- [5] Y. Xu, J. Wang, Z. Chang, B. Ding, Y. Wang, L. Shen, C. Mi, H. Dou and X. Zhang, *CHEMISTRY, A European Journal*, **22**: 4256-4262 (2016).

- [6] B. You, F. Kang, P.Q. Yin, Q. Zhang, *Carbon*, 103:9-15 (2016).
- [7] Y. Song, J. Yang, K. Wang, S. Haller, Y. Wang, C. Wang and Y. Xia, *Carbon*, **96**: 955-964 (2016).
- [8] Y. Wang, F. Su, C. D. Wood, J. Y. Lee and X. S. Zhao, *Ind. Eng. Chem. Res.*, **47**:2294 (2008).
- [10] J. Zeng, Q. Cao, B. Jing and X. Peng, *RSC Adv.*, **6**:15320-15326 (2016).
- [11] Y. Chen, Z. Gao, B. Zhang, SC. Zhao and Y. Qin, *J. Power Sources*, **315**: 254-260 (2016).
- [12] S. Suresh Balaji, A. Elavarasan and M. Sathish, *Electrochimica Acta*, **200**:37-45 (2016).